

Abandonment study Nedmag caverns

Cavern squeeze modeling and geophysical analysis of brine permeation and containment



Prepared by: Well Engineering Partners B.V.
Hoogeveen

Author: dr.ir. A.J.H.M. Duquesnoy

Verification: ir. A. Nagelhout

Version: 2 final

Publication date: 31 March 2015

Agreed: F. Goorman, Nedmag T&B development



Contents

Management summary.....	2
1 Introduction.....	3
2 Global lithological data and cavern model.....	5
3 Initial relative squeeze modeling.....	6
4 Two-branch squeeze model.....	9
5 Cavern roof stability analysis.....	13
6 Cavern system integrity after definite abandonment.....	17
7 WEP squeeze model revision.....	20
7.1 New permeation concept for sealed brine-filled caverns.....	20
7.2 Balanced brine squeeze and migration model.....	20
8 Migrated brine containment and confinement.....	23
8.1 Integrally coupled balanced brine squeeze and flow process.....	23
8.2 New coupled balanced model for strong squeeze drive.....	24
8.3 Extended balanced two-branch squeeze model.....	25
8.4 Lower Bunter containment analysis.....	26
8.5 Brine migration confinement by Solling claystone.....	27
9 Sensitivity analysis.....	28
9.1 Inventory of epistemic uncertainties.....	28
9.2 Inventory of stochastic uncertainties.....	29
9.3 Likelihood and reliability of results obtained.....	29
10 Assessment of bulking factors from a literature survey.....	37
11 Summary of principal abandonment modeling results.....	40
12 Production and abandonment scenarios.....	41
12.1 Scenario 1: Nedmag Winningsplan 2013.....	41
12.2 Scenario 2: WEP proposal.....	42
12.3 Concluding remarks.....	42
13 References.....	44
Attachment 1: Stratigraphy of VE and TR subsurface.....	46
Attachment 2: Map of Nedmag cavern system.....	47
Attachment 3: General cavern system model.....	48
Attachment 4: Bulked volume model output.....	49
Attachment 5: Modeled squeeze volumes for production phase.....	50
Attachment 6: Two branch relative squeeze contributions.....	51
Attachment 7: Free and squeeze volumes for production and pre-abandonment phase.....	52
Attachment 8: Equivalent circular span of 3b cavern roofs.....	53
Attachment 9: Salt barrier between 3b caverns and Lower Bunter formation.....	54
Attachment 10: Roof composition near VE-1 casing shoe.....	55
Attachment 11: Cavern situation VE-1 after abandonment.....	56
Attachment 12: Halite permeability as a function of effective fluid pressure.....	57
Attachment 13: Cross section through wells VE-2, VE-1 and TR-7.....	58
Attachment 14: Sonar measurement in 3b cavern TR-6.....	59
Attachment 15: Mohr-Coulomb stability criterion for disc-shaped roofs.....	60

Management summary

On 3 October 2014 the Minister of Economic Affairs has approved of a modified production plan (Winningsplan 2013) under certain conditions, amongst others article 5, stating that Nedmag investigates and reports before 1 July 2015 the best practices to definitely abandon the caverns.

This study presents salt creep and brine permeation modeling for estimating the evolution of the Tripscompagnie (TR) & Veendam (VE) cavern system, using Nedmag's BDS data (Brine Data System) as a reference. The development of the free brine volume in the system is modeled aiming at a robust cavern abandonment strategy with minimal free brine volume left in the system at the moment of cavern sealing and definite field abandonment. A scenario approach is adopted and consequences are estimated over a 100 year period after abandonment. Essential items investigated are roof and wellbore stability, brine permeation from the cavern system into the overlying formations and the occurrence of land subsidence. Also, a sensitivity analysis regarding the effect of uncertainties in many modeling parameters is included.

The main results obtained are the following:

- Free-brine bleed-off at reduced cavern pressures as proposed in the Winningsplan 2013 in preparation of definite cavern sealing is not needed for controlling long-term land subsidence.
- During all operational phases roof stability is warranted for all caverns.
- Under abandonment conditions an integrally coupled model is required between cavern convergence, brine permeation and hydraulic roof capacity and the containment properties of the overlying permeable Lower Bunter mudstone.
- The Zechstein salt roof is not hydraulically tight anymore under abandonment conditions, but the Zechstein roof integrity and the containment capacity of the overlying Lower Bunter mudstone are warranted.
- The huge containment capacity of the Lower Bunter mudstone makes the overlying, very tight Solling claystone redundant as ultimate confinement zone and environmental barrier.
- A literature survey on bulking factors indicates that the applied bulking factor of 1.10 in the Winningsplan 2013 is not supported by the collected data so far. In case of coarse insoluble material a conservative bulking factor of 1.3 seems appropriate and in case of finely-distributed insoluble components 1.4 or more should be applied

WEP has developed an alternative scenario for field abandonment, which also matches with BDS data. The main characteristics of this so-called *no bleed-off* scenario are:

- Active brine production can be continued until end 2026. Land subsidence is expected to be circa 61 cm. The reference date for zero subsidence is July 1993.
- The total cavern field is subjected to a hard shut-in operation at the beginning of 2027 without pre-abandonment period of bleeding-off free brine.
- After 100 years of definite abandonment, the expected land subsidence is circa 63 cm.

As a concluding remark, this study has shown that BDS data and pertinent figures in the Winningsplan 2013 for strategies of future brine production and cavern abandonment should be viewed with prudence.

1 Introduction

On 26 March 2013 NEDMAG Industries Mining & Manufacturing B.V. in Veendam (Nedmag) has requested the Minister of Economic Affairs for approval of a modified production plan for potassium and magnesium salts (Winningsplan 2013q). The plan announces a study into best practices to abandon the caverns after final production stop (ref.1).

On 3 October 2014 the Minister of Economic Affairs has approved of the modified plan under certain conditions, amongst others article 5, stating that Nedmag investigates and reports before 1 July 2015 the best practices to definitely abandon the caverns.

Nedmag already requested WEP on 16 April 2012 to perform a comprehensive study on the final abandonment of the wellhead clusters Veendam (WHC-1) and Tripscompagnie (WHC-2). The study should comprise the modeling of a reference cavern for both a pre-abandonment cavern squeeze phase and the definite abandonment phase, and the analysis of the cap rock behavior above the caverns.

After a pre-feasibility study of WEP and the presentation of a study proposal on 17 August 2012 to State Supervision of Mines and TNO-Utrecht the following aim of the study has been corroborated:

- É Define a multi-salt squeeze model to estimate the evolution of the Tripscompagnie (TR) & Veendam (VE) cavern system, using Nedmag's BDS data (Brine Data System) as a reference.
- É Determine the development of the free brine volume in the system and advice on cavern abandonment strategy to minimize the free brine volume at production life end, and to prohibit that isolated free brine volume is left in individual caverns.
- É Use a scenario approach and calculate effects over a 100 year period for comparison of different scenarios.
- É Estimate the brine permeation into the salt roof after cavern sealing and abandonment, and perform a risk analysis on:
 - a) roof and wellbore stability,
 - b) brine leakage from the cavern system into the overlying formations,
 - c) land subsidence.

A second discussion with State Supervision of Mines and TNO-Utrecht has taken place on 16 May 2014, during which a sensitivity analysis regarding the most critical modeling parameters is asked for, including an assessment of the variance in the final results. The requested items also form part of the present study.

Short preview of progression in salt creep modeling in this study

Chapter 3 introduces cavern squeeze modeling based on non-linear relative salt creep. Also, a bulked volume model is introduced for splitting total brine, left in the system after cavern convergence, into freely movable and bound brine.

Chapter 4 shows that a two-branch squeeze model should be used for all cavern process phases (production, pre-abandonment bleeding-off and definite cavern abandonment) to get useful squeeze results. Thus, earlier relative non-linear modeling has become obsolete.

Chapters 6 demonstrates that in the final abandonment phase purely stand-alone two-branch squeeze modeling, presented in chapter 4, is also not adequate enough. There is a mismatch between the autonomously determined brine squeeze volume and roof permeation capacity.

Chapter 7 introduces a balanced brine squeeze and migration model. Essential here is the introduction of an effective brine overpressure relative to local lithostatic pressures at roof level that slows down cavern salt creep and increases the Zechstein roof permeability

Chapter 8 elaborates on the understanding of the physical prerequisite for balancing the brine flow as a result of salt creep and the flow capacity of the rock layers in and above the cavern roof. It presents a coupled balanced model for strong squeeze drive under abandonment conditions. At the same time coupled Darcy flow modeling controls hydraulic equilibrium between permeating brine and the containment capacity of the Lower Bunter mudstone above the roof.

2 Global lithological data and cavern model

Nedmag produces the magnesium salts from the Zechstein III mixed salt formation by means of 13 wells. At surface 4 wells are situated at the WHC-1 cluster (VE-wells) and 9 wells at the WHC-2 cluster (TR-wells). In attachment 1 the stratigraphy is schematically shown. Usually, a lower and upper cavern per well have been leached, separated by a halite layer of circa 40 m thickness. In attachment 2 the position of the 13 wells is depicted at the level of the Zechstein salt formation. Wells TR-8 and TR-9 have no upper cavern. Well VE-1 has no lower cavern. Most VE and TR wells are hydraulically connected, predominantly via the lower caverns in view of the observed pressure differences at the wellheads. To date, exceptions are well VE-1 that has no lower cavern and the recent well TR-9 that has a lower cavern still disconnected from other caverns. Also, the lower caverns of VE-2 and VE-3 are mutually connected, but still disconnected from other caverns.

WEP has developed a general model of the cavern system that is shown in attachment 3. The model consists of three mining cuts and presumes a prevalence of residuals in the lower cavern section. The overburden rock is divided into containment and confinement zones with respect to cavern brine possibly migrating through the Zechstein rock salt roof. A global lithological model has been derived for the three cuts, using data from the 13 wells. The result is given in Table 1. The thickness of 63.4 m for the ZE-III 2a halite layer is a calculation artefact, resulting from taking the average of the data of the individual wells.

	<u>Formation</u>	<u>From(m NAP)</u>	<u>To(m NAP)</u>	<u>Thickness (m)</u>	<u>Medium Depth(m NAP)</u>	<u>Carnallite %(v/v)</u>	<u>Bischofite %(v/v)</u>	<u>Kieserite %(v/v)</u>	<u>Halite % (v/v)</u>	<u>Sylvite % (v/v)</u>
CUT 3	ZE-III 2b/3b	1561,2	1603,8	42,6	1582,5	38,3	0,0	8,7	52,7	0,2
	ZE-III 2a	1607,6	1671,0	63,4	1639,3					
CUT 2	ZE-III 1b car/bis	1671,0	1719,0	48,0	1695,0	25,0	28,0	5,9	40,8	0,3
CUT 1	ZE-III 1b car	1719,0	1732,2	13,1	1725,6	48,5	0,8	5,8	46,7	0,8

Table 1: Lithological composition, layer thickness and depth for the three cuts of the general cavern system model (ref. Corrected Two-b Sq.model VE+TR v.1).

However, in all following investigations and calculations *individual* TR and VE cavern data have been commonly used (depth, thickness and ore composition per model cut)

3 Initial relative squeeze modeling

As a starting point, WEP has applied its standard squeeze model with non-linear *relative* salt creep to the Nedmag field situation. The model has been applied to three cavern process phases: regular production, pre-abandonment bleed-off, and definite sealing and abandonment of the complete cavern field.

During the operational and bleed-off phases the pressure deficit P of the cavern brine relative to the ambient salt formation pressure is more than 5 MPa. Then, as a first order approach, a simple Norton-Hoff formula is sufficient for describing the salt creep process, causing cavern convergence and squeezing out cavern brine. The non-linear relative salt creep model uses reference squeeze data observed in the halite brine producing cavern BAS-1, operated by esco/Frisia Zout B.V (Frisia) in Harlingen (ref.2). The reference data have been released by Frisia for use in this study and are summarized in Table 2.

Halite salt @ 2760 m depth		BAS-1 ref-data	
Reference squeeze rate	$V_{sq,ref}$	700.8	[m ³ /day]
Activation energy	Q/R	6201	[K]
Salt temperature	T_{ref}	376	[K]
Pressure difference	P_{ref}	227	[bar]
Cavern volume	V_{ref}	424 000	[m ³]
Non-linear exponent	n_1	3.6	[-]

Table 2: Reference data on stationary squeeze process in Frisia cavern BAS-1.

Using the reference data of Table 2 the squeeze volume V_{sq} [m³/day] is calculated per model cut as follows:

$$\Delta V_{sq} = M_{salt} \cdot V_{sq,ref} \cdot \left[\frac{e^{-\frac{Q}{RT}}}{e^{-\frac{Q}{RT_{ref}}}} \right] \cdot \left(\frac{\Delta P}{\Delta P_{ref}} \right)^{3.6} \cdot \left(\frac{V}{V_{ref}} \right)$$

Where: M_{salt} = mobility factor for differently creeping salt types,
 T = temperature [K], with: $T = 273 + 10 + 0.033 \times \text{Depth [m]}$,
 V = free volume [m³] of each of the three squeezing volume cuts per cavern.

For the Nedmag case parameter M_{salt} is introduced in order to incorporate different salt creep properties, where $M_{bischofite} > M_{carnallite} > M_{halite}$. According to a Nedmag rule of thumb the respective mobility factors are $M_b:M_c:M_h = 100:10:1$ (ref.3).

WEP has developed a brine volume model consisting of two parts:

1. *Bulked volume model* for splitting the BDS defined total system brine volume into two fractions: bound and freely movable brine.
2. *Non-linear salt creep model* for calculating the squeeze rate of the free brine fraction in the cavern system.

Bulked volume model

BDS volumes for the period 2010-2026 have been applied to match the squeeze volumes of the WEP bulked volume model with BDS squeeze volumes. WEP has slightly revised some BDS data to get a good match:

- Dissolved and precipitate BDS volumes have been split and assigned to 3 cuts
- A correction factor is applied to the BDS squeeze volumes ($\pm 2\%$) to get a better match between BDS and WEP squeeze volumes.

The calibrated WEP model splits the remaining system brine after squeeze into free brine volume and bound brine volume. In attachment 4 the output of the bulked volume model is presented. The free brine volume is determined by the bulking factor. The base case applies to a bulking factor $BF = 1.10$ for insoluble material (inert rock and precipitated salts), adopted from the recently approved ~~W~~Winningsplan 2013q(ref.1). Yearly free-volume decay is faster for higher bulking factors and at the end of 2026 no free brine volume is left for $BF=1.14$. Attachment 5 shows the good agreement between bulked volume model squeeze and BDS.

Non-linear salt creep model

WEP starts the squeeze volume calculations at the beginning of 2012. The three salt mobility factors in the model have been iteratively optimized to achieve the best match to the BDS prescribed squeeze volumes. The following optimal mobility factors have been obtained:
 $M_{\text{halite}} = 1$; $M_{\text{carnallite}} = 54$; $M_{\text{bischofite}} = 216$, shortly denoted 1 - 54 - 216.

The BDS squeeze volume calculations used to start in July 1993, although magnesium brine production actually started in 1972. Until July 1993 brine production took place mainly in a high-pressure mining mode with little cavern convergence. In the Nedmag ~~W~~Winningsplan 2013qit is supplementary estimated that from the start of brine production in 1972 until July 1993 an additional squeeze brine production amounting to circa 0.5 million m^3 may have been effectuated. However, in line with the primary approach in the Winningsplan 2013 the present study takes July 1993 as reference date for cumulative squeeze volume calculations.

During the production period 2012-2026 the expected operational pressure deficit amounts to 67.5 bars re lithostatic pressure at the TR-7 shoe at a depth of 1463 m TV NAP. In the WEP calculations depth, thickness and ore composition pertinent to individual caverns and cuts are applied. The actually dissolved ore volumes and available free brine volumes specific to each cavern and each model cut are unknown. Therefore, the WEP squeeze calculations start with equal average free volumes for each cavern. In January 2012 these values are as follows: cut 1 #10800 m^3 , cut 2 #145883 m^3 , cut 3 #120445 m^3 . No free volumes are assigned to cuts 1 and 2 of well VE-1, and to cut 3 of wells TR-8 and TR-9. Attachment 5 shows the good agreement between the non-linear model squeeze volumes and BDS defined volumes.

For a land subsidence limit of 65 cm in the deepest point of the subsidence bowl Nedmag expects that the corresponding cumulative squeeze volume amounts to 10.5 million m^3 . So, according to the Nedmag Winningsplan 2013 the most likely criterion is approximately 6 cm land subsidence per million m^3 squeeze volume. In practice, the active production phase should stop before the squeeze volume limit and corresponding subsidence limit are reached in order to reserve room for field abandonment operations.

Pre-abandonment bleed-off phase

According to the Winningsplan 2013 a bleed-off phase is planned before final field abandonment, aiming at bleeding off more than 90% of the remaining free brine volume. In this phase WEP modeling is not controlled by interfering BDS data.

The planned bleed-off is as follows:

- Stage 1: 4 years bleeding off mainly cut-2 bischofite brine at a sub-lithostatic pressure of 100 bars at reference depth 1549 m TV (= average shoe depth of cavern system);

- Stage 2: next 6 years bleeding off mainly cut-3 carnallitic brine at a sub-lithostatic pressure of 125 bars.

In order not to exceed the total squeeze limit volume of 10.5 million m³ the bleed-off phase should start at the beginning of 2021 at a cumulative squeeze volume of 8.36 million m³. All bleed-off volumes are calculated relative to an average temperature of 337.5 K (64.5 °C). In Table 3 the WEP-model derived free volumes have been summarized per cavern cut before and after bleeding off.

Free Volumes at start of bleed-off (m ³) in 2021 (13 caverns)		Free Volumes at end of bleed-off (m ³) in 2031 (13 caverns)	
Cut 3	931.314	Cut 3	219.484
Cut 2	1.317.078	Cut 2	1.234
Cut 1	0	Cut 1	0
Total	2.248.392	Total	220.718

Table 3: Free volumes at start and finish of the pre-abandonment bleed-off phase obtained by means of the non-linear-squeeze only model.

Final abandonment phase

It is assumed that the pressure at the cavern field leak-off point will instantaneously increase to lithostatic conditions as soon as the final abandonment phase starts in 2031. The cavern field leak-off point is situated at the VE-1 shoe at a depth of 1365 m TV NAP. A lithostatic gradient of 0.22 bar/ m is applied. The total free volume left in the abandoned cavern field is circa 0.22 million m³. The pressure difference build-up below the leak-off point is 0.088 bar/m for carnallitic brine (s.g. 1.32 tons/m³) and 0.083 bar/m for bischofite brine (s.g. 1.37 tons/m³). Any squeeze volume is assumed to directly permeate into the overburden via the leak-off point, thus permeation volume equals squeeze volume.

The pressure deficit in Cut 3 (carnallitic layer) at a medium depth of 1582.5 m is $P_{\text{aband}} = 19.1 \text{ bar} [(1582.5-1365)*0.088]$, with $T = 335 \text{ K}$ and average $M_{\text{salt}} = 21$. The M_{salt} value is calculated as follows: Cut 3 is subdivided per cavern into layers with varying thickness and different salt compositions; per individual layer the salt mobility is calculated applying the 1 - 54 - 216 relative mobility for halite (and kieserite)-carnallite-bischofite salts; next, all layer mobility of all caverns are averaged with layer thickness as a weighing factor.

The pressure deficit in Cut 2 (bischofite layer) at a medium depth of 1695 m is $P_{\text{aband}} = 28.4 \text{ bar} [19.1+(1695-1582.5)*0.083]$, with $T = 339 \text{ K}$ and average $M_{\text{salt}} = 78$.

The calculated squeeze and permeation volume in the first year of abandonment is $V_{\text{sq}} = 57 \text{ m}^3/\text{year}$, decreasing to $54 \text{ m}^3/\text{year}$ after 100 years, with cumulative squeeze volume of circa 5500 m³ after 100 years. The volumes have been calculated for $T_{\text{average}} = 337.5 \text{ K}$ and result from applying a relative non-linear squeeze model only. However, as shown below linear squeeze processes should be taken into account as abandonment standard (see Chapter 4).

4 Two-branch squeeze model

In this chapter a two branch squeeze model with linear and non-linear salt creep is presented. New model coefficients have been derived and the model has been generally applied to the three cavern process phases.

The two-branch cavern squeeze per time unit is determined according to the formula:

$$\frac{dV}{V} = \sqrt{3} \left(\frac{\sqrt{3}}{n_1} \Delta P \right)^{n_1} \cdot A_1 \cdot e^{-\frac{Q_1}{RT}} + \sqrt{3} \left(\frac{\sqrt{3}}{n_2} \Delta P \right)^{n_2} \cdot A_2 \cdot e^{-\frac{Q_2}{RT}}$$

Where: V = squeeze volume [m³/day]
 V = free brine volume in cavern [m³]
 P = pressure deficit relative to the local lithostatic pressure [MPa]
 n₁ = non-linear exponent >1
 A₁ = non-linear model coefficient [1/day.MPa^{n₁}]
 Q₁/R = activation energy non-linear salt creep [K]
 T = temperature in cavern [K]
 n₂ = linear exponent = 1
 A₂ = linear model coefficient [1/day.MPa^{n₂}]
 Q₂/R = activation energy linear salt creep [K].
 R = gas constant = 8.3143 10³ J/K

Derivation of linear model coefficient A₁

The model coefficient A₁ is derived from the Frisia reference data of Table 2. Inserting the data into the non-linear branch of above formula yields: A₁ = 2.54 /day.MPa^{3.6}. This value relates to the creep of rock salt. For other salts the coefficient is A₁ = 2.54 M_{salt} /day.MPa^{3.6}.

Derivation of linear model coefficient A₂

Coefficient A₂ is derived on the basis of uniaxial creep data for bischofite (ref.4). For P < 2 MPa and T = 333 K, it was observed: d/dt (ax) = 0.61 10⁻⁸ (P)^{1.5} [1/s], with n₂ = 1.5 (quasi-linear creep). Then, the volumetric relationship of the linear model component becomes:

$$dV/V = \sqrt{3} \left(\frac{\sqrt{3}}{1.5} \right)^{1.5} d/dt(ax) = 2.15 (0.61 \cdot 10^{-8} (P)^{1.5}) \cdot 2.15 (P)^{1.5} A_{2b} e^{-Q/RT} [1/s].$$

Converting seconds to days (86400 s/ day) yields: A_{2b} e^{-Q/RT} = 0.61 10⁻⁸ 86400 = 0.53 10⁻³ [1/day.MPa^{1.5}]. The value for A_{2b} depends on the activation energy Q of bischofite, for which values between 8.8 and 10 (± 4.9) kcal/mol were reported (ref.4), where 1 kcal/mol = 4.186 10³ J/Mol. For Q = 10 kcal/mol and T = 333 K it follows Q/R = 5035 K, Q/RT = 15.1 and A_{2b} = 1955 /day.MPa^{1.5}. For halite it follows A₂ = A_{2b}/M_{bischofite} = A_{2b}/216 = 9.0 /day.MPa^{1.5}. Since linear creep is predominant in situations for which P < 2 MPa, it is approximately right to apply the same A₂ value for the strict linear branch of the two-branch squeeze model, where n₂ = 1.

Deltares (ref.5) derived A₂ values for halite under Frisia mining conditions with T= 376 K and Q/R= 6201 K and found for low linear creep A₂ = 14.5 /day.MPa and for high linear creep A₂ = 74.1 /day.MPa. Converted to a Nedmag average cavern temperature T = 337.5 K (64.5 °C) the low and high A₂ values become 2.15 and 11.0 /day.MPa, respectively. The value A₂ = 9.0

/day.MPa (for halite), indirectly derived from bischofite creep data at $T = 333$ K, seems to be a realistic compromise.

Relative contribution of linear and non-linear salt creep

In attachment 6 the trade-off between linear and non-linear salt creep as a function of pressure deficit P is presented using $A_1 = 2.54$ /day.MPa^{3.6} and $A_2 = 9.0$ /day.MPa, with $Q/R = 6201$ and $T = 333$ K (60 °C). In the operational phase the reference pressure deficit P_{ref} at the TR-7 shoe at a depth of 1463 m TV is 67.5 bars. At the field's average shoe depth of 1549 m TV this corresponds to a maximum pressure deficit P of 75 bars [(1549-1463)*(0.22-0.132) +67.5]. The relative contribution of linear creep is still significant (> 30%) at these pressure deficits. In the pre-abandonment phase P ranges from 100 to 125 bars and, then, mainly non-linear creep is effective (about 90% non-linear and 10% linear). In the abandonment phase P ranges between 19 bars (Cut 3) and 28 bars (Cut 2), thus, in that phase mainly linear creep is active (about 90% linear and 10% non-linear).

It is concluded that the two-branch creep model should be generally applied in all cavern process phases to get accurate squeeze results.

Calibration of two-branch squeeze model

Since in the operational phase the average pressure deficit P is about 75 bars, the relative contribution of linear salt creep will evidently enhance the squeeze volumes by circa 30% relative to the non-linear basic model. In order to again achieve squeeze volumes matching the production plan and BDS volumes, the salt mobility factors and consequently the A_2 value have been varied iteratively for the operational phase condition.

New optimum relative mobility factors M_{salt} for halite-carnallite-bischofite have been achieved, being equal to **1 - 40 - 160**, respectively (cf. non-linear case 1 - 54 - 216). Remarkably, the mobility ratio between carnallite and bischofite remains identical for both non-linear and two-branch squeeze modeling, namely 1 to 4.

The corresponding optimum A_2 coefficient for halite appears to be $A_2 = 13.9$ /day.MPa = $0.161 \cdot 10^{-3}$ /s.MPa, slightly larger than the above literature derived values.

During the production phase the two-branch model output is identical to the non-linear model output as shown before in attachment 5, because all volumes are BDS controlled. The salt activation energies applied are $Q_1/R = Q_2/R = 6201$ K.

Effect of different bulking factors

As shown in attachment 4 the bulking factor has a significant impact on the free brine volume available in the course of time for cavern convergence and squeeze. In the base case of the modified production plan (ref.1) a bulking factor of 1.10 has been presumed with an average standard pressure deficit of 67.5 bars (at TR-7 shoe).

If a bulking factor deviating from 1.10 is taken into account, the squeeze volumes produced by the WEP model start grossly deviating from the BDS data, in a positive sense for lower bulking factors (more free volume) and in a negative sense for higher bulking factors (less free volume). The way of correcting for these deviations and to comply with the BDS data is to vary the brine pressure deficit during the regular production phase. In Table 4 examples of the required pressure variations are shown as a function of the bulking factor. The bulking factor also determines the year of starting the bleed-off procedure in order not to exceed 10.5 million m³ total squeeze volume up to definite cavern abandonment.

Year	Sub-lithostatic pressures at TR-7 shoe (bar)		
	BF = 1.11	BF = 1.10	BF = 1.09
2012	67,5	67,5	67,5
2013	67,5	67,5	65,5
2014	67,5	66,5	63,5
2015	67,5	65,5	61,5
2016	67,5	64,5	59,5
2017	67,5	64,5	57,5
2018	67,5	65,5	57,5
2019	68,5	66,5	58,5
2020	70,5	67,5	59,5
2021	72,5	68,5	Start bleed off
2022	77,5	Start bleed off	
2023	82,5		
2024	Start bleed off		

Table 4: Model sub-lithostatic pressure variations required for compliance with BDS squeeze volumes for different bulking factors BF. The bulking factor also determines the start year of the bleed-off phase.

Bleed-off phase

In the bleed-off phase the two-branch squeeze model provides results different from the basic non-linear model. At higher pressure deficits the two-branch model calculates less squeeze volume because of a reduced contribution of the linear component. Furthermore, the salt mobility factors M are reduced as compared to the basic non-linear model. Consequently, in order to arrive at circa 10.5 million m^3 cumulative squeeze volume at the start of definite cavern abandonment the pressure deficit during the bleed-off stages has to be increased by an extra 10 bars. The remaining free volume in the base case is 0.17 million m^3 compared to 0.22 million m^3 for the non-linear model (see Table 3).

The effect of different bulking factors on the model output compared to the base case has been investigated. In Table 5 the results of the two-branch model output are summarized up to and including the first 100 years after final field abandonment and compared to the figures presented in the approved Winningsplan 2013.

For the base case, in which the bulking factor is 1.10, the decrease in free volume per cavern cut in the course of time is graphically shown in attachment 7A and the cumulative squeeze volume increase is shown in attachment 7B.

The most obvious difference between the non-linear and two-branch squeeze models occurs during the definite abandonment phase. The two-branch squeeze volume calculated in the first year of abandonment is $V_{sq} = 477 m^3/year$, decreasing to $333 m^3/year$ after 100 years, with a cumulative squeeze volume of circa 39600 m^3 after 100 years. These volumes are about a factor 7 larger than for the basic non-linear model presented in chapter 3.

	Winnings-plan 2013	Bulk.f. = 1.10 (base case)	Bulk.f.= 1.09	Bulk.f.= 1.11
Year start bleed-off	2024	2022	2021	2024
Total squeeze vol. at start bleed-off (Mm ³)	9.5	8.44	7.95	8.91
Remaining free brine vol. (Mm ³)	1.0	2.16	2.59	1.59
Bleed-off period (years)	4-5 (2 stages)	10 (2 stages)	10 (2 stages)	10 (2 stages)
Pressure difference during bleed-off stages (bar)	Not specified	1 st : 110 2 nd : 135	1 st : 110 2 nd : 135	1 st : 110 2 nd : 135
Remaining free brine vol. after bleed-off (Mm ³)	0.0	0.17	0.19	0.14
Total squeeze vol. (from 1993 until abandonment) (Mm ³)	10.5	10.43	10.35	10.36
Permeation in first year abandonment (m ³ /yr)	---	477 (2.8š)	538 (2.8š)	402 (2.8š)
Permeation after 100 years abandonment (m ³ /yr)	---	333	374	283
Permeation volume during first period of 100 years (Mm ³)	---	0.040	0.045	0.033

Table 5: Data published in the Winningsplan 2013 with regard to the bleed-off phase. The corresponding two-branch squeeze model output is given for three different bulking factors. Permeation in 1st abandonment year is a function of post bleed-off free volume. Mm³ means million m³.

Application of two-branch model in no bleed-off case

The Winningsplan 2013 is designed for limiting land subsidence caused by salt creep and cavern convergence to 65 cm, with zero reference date July 1993. The relation between cumulative squeeze volume and land subsidence in the deepest point of the bowl is almost linear. Land subsidence in the deepest point as a function of cavern squeeze is typically circa 6 cm per million m³ squeeze volume. To date, this number appears to be stable.

Assuming a subsidence horizon of 100 years, brine production could be continued until 2025 with the total squeeze limited to 9.43 million m³ (from July 1993). Subsequently, the cavern system is subjected to *hard shut-in* without bleeding-off phase. The remaining free brine volume is 1.85 million m³ at the start of the definite abandonment in 2025. The two-branch model calculates a significant permeation rate of about 31300 m³ in the first abandonment year, with a cumulative squeeze volume of 1.17 million m³ in 100 years after hard shut-in. After 100 years the total squeeze volume as from July 1993 amounts to 10.6 million m³. The expected land subsidence 100 years after abandonment is 63.6 cm (in 2125). Whether the no bleed-off case is realizable geophysical, indeed, is further investigated and discussed in chapters 7 and 8.

5 Cavern roof stability analysis

In this chapter the stability of the cavern roofs is investigated for the process phases after regular production stop. Focus is on roof stability of the upper 3b-sections of the VE and TR caverns. Until 1995 Nedmag has controlled cavern roof shape and roof area with an oil blanket. In 1995 Nedmag has removed the oil blankets from the caverns. The cavern roofs are naturally protected against unwanted upward leaching by the halite layer on top of the bischofite and carnallite salt layers (ref.6). Since 2000 Nedmag has ceased injecting dissolution water in the upper 2b/3b caverns, except for TR-7, where injection stopped in 2010. Henceforth, operations are focused on water injection and brine production at the level of the lower 1b sections.

Inventory of present status of roof conditions in 3b-section

In this study the roof areas are represented as circular shapes in order to get comparable uniform data on the cavern roofs.

In the BDS system no discrimination is made between the carnallite volumes dissolved from the 2b or 3b sections. From specifications of water injection depths the water volumes injected in the 2b or 3b sections have been derived. For most caverns it is uncertain whether the injected water in the 2b section has dissolved carnallite in that section only. The water might have (partially) dissolved carnallite in the 3b section as well. For a very conservative assessment of 3b roof spans it is assumed that all injected water has solely dissolved carnallite in the 3b section, which yields the maximum possible span of 3b cavern roofs. In Table 6 the potentially dissolved carnallite volumes per section and for the two sections in total are summarized for the situation end 2014 (ref.7). In wells TR-8 and TR-9 no upper 2b/3b caverns have been dissolved.

Cavern	Carnallite				
	2b dissolved volume (m ³)	2b content (vol. %)	3b dissolved volume (m ³)	3b content (vol. %)	2b + 3b dissolved volume (m ³)
VE-1	182357	47	63058	47	245415
VE-2	0	38	158493	45	158493
VE-3	215907	44	28779	40	244686
VE-4	214391	49	0	50	214391
TR-1	189111	37	62033	45	251144
TR-2	41929	31	215617	50	257546
TR-3	184178	52	195937	61	380115
TR-4	17565	45	274535	50	292100
TR-5	223161	52	0	56	223161
TR-6	120990	45	69095	56	190085
TR-7	920255	56	0	62	920255

Table 6: Dissolved volumes and volumetric content of carnallite in 2b and 3b cavern sections.

The 3b roof spans are ultimately determined by the affected total rock volume and the thickness of the dissolved 3b carnallite layer. The affected volumes are inversely dependent on the carnallite content in the 2b/3b sections. The average carnallite content per cavern section, adopted from core analyses and logs, is also shown in Table 6.

Using the data from Table 6 minimum roof spans of 3b caverns are calculated from 3b dissolution volumes alone and maximum roof spans from the summed 2b/3b dissolved volumes. Table 7 summarizes the pertinent input data and the resulting diameters of

equivalent circular roofs. In attachment 8 the minimum and maximum roof diameters are graphically shown.

Cavern	Volume 3b min affected (m ³)	Volume 3b max affected (m ³)	3b layer thickness (m)	Minimum roof diameter (m)	Maximum roof diameter (m)
VE-1	134166	522160	15	107	211
VE-2	352207	352207	30	122	122
VE-3	71948	611715	9	101	294
VE-4	0	428782	12	0	213
TR-1	137851	558098	12	121	243
TR-2	431234	515092	8	262	286
TR-3	321208	623139	11	193	269
TR-4	549070	584200	8	296	305
TR-5	0	398502	10	0	225
TR-6	123384	339438	8	140	232
TR-7	0	1484282	12	0	397

Table 7: Minimum and maximum circular roof diameters for cavern sections 3b based on affected rock volume and layer thickness.

Other important aspects for cavern roof stability are the composition and thickness of the competent roof layer. In Table 8 an inventory is given of all data relevant to roof stability and integrity (refs.7, 8).

Cavern	VE-1	VE-2	VE-3	VE-4	TR-1	TR-2	TR-3	TR-4	TR-5	TR-6	TR-7
Average roof depth 3b cavern (mTV NAP)	1439	1414	1599	1480	1539	1616	1572	1762	1601	1676	1476.5
Bottom Trias (mTV NAP)	1344	1322	1495	1384	1464	1510	1469	1655	1490	1566	1397.5
Casing shoe 2000 (mTV NAP)	1365	1398	1588	1458	1538	1612	1602	1764	1588	1672	1480
Casing shoe 2010 (mTV NAP)	1365	1398	1588	1458	1538	1612	1544	1759	1588	1624.5	1463
Total ZE roof thickness (m)	95	92	104	96	75	106	103	107	111	110	79
Distance shoe - Trias (m)	21	76	93	74	74	102	75	104	98	58.5	65.5
ZE roof composition:											
1. Anhydrite in ZE-IV (m)	5	2	2	2	2	11	7	7	8	2	3
2. Bedded clayey halite (m)	49	56	43	53	23	22	21	15	19	14	7
3. (Almost) pure halite (m)	41	34	59	41	50	73	75	85	84	94	69

Table 8: Relevant data of 3b cavern roofs for rockmechanical stability and hydraulic integrity.

It is assumed that the Zechstein formation is providing the roof strength, as well as the hydraulic integrity. The integrity is delivered by the extremely low porosity and permeability of the salt. The overlying Lower Bunter sandstone, composing the bottom of the Trias period, is permeable and clayey sandstone, not contributing to the cavern roof strength and hydraulic integrity. The robustness of hydraulic integrity is primarily determined by the distance between the last cemented casing shoe and bottom Trias.

Calculation of roof stability

The roof stability is analysed by means of the conventional Mohr-Coulomb failure criterion. The roof is considered as a circular plate, which is laterally clamped and vertically loaded (ref.9). The plate is loaded in tension force mode. The minimally required roof thickness for

long-term stability is calculated according to the following failure criterion, the derivation of which is given in attachment 15:

$$h_{\text{roof}} > 0.5 R \cdot \frac{1}{\sin \alpha} \left\{ \frac{2 \cdot P \cdot (1 - \sin \alpha)}{2C \cdot \cos \alpha + P_{\text{cav}} \cdot (1 + \sin \alpha)} \right\}$$

Where: R = radius of circular roof plate [m]

^a P = brine pressure deficit at the roof relative to the local lithostatic pressure [MPa]

α = friction angle of roof salt rock [°]

C = cohesion of roof rock salt [MPa]

P_{cav} = brine pressure at cavern roof [MPa].

The Zechstein roofs are composed of halite, clayey halite and some anhydrite. The strength of the anhydrite layers is taken identical to the halite strength. The applied rockmechanical properties are for halite C = 3.3 MPa, α = 33°; for clayey halite C = 3.5 MPa, α = 26° (ref.10).

The roof stability is investigated for three pressure deficit regimes relative to the system's reference depth of 1549 m:

1. Production phase: ^a P = 7.5 MPa
2. Bleed-off phase 1: ^a P = 11.0 MPa
3. Bleed-off phase 2: ^a P = 13.5 MPa.

The pressure deficit gradient in the carnallitic brine column amounts to 0.0088 MPa/m. The pressure deficit at 3b cavern roof depth is separately calculated for each cavern.

Minimum thickness Hmin for cavern roof	VE-1	VE-2	VE-3	VE-4	TR-1	TR-2	TR-3	TR-4	TR-5	TR-6	TR-7
Max. roof span 3b cav.(m)	211	122	294	213	243	286	269	305	225	232	397
1. Pdeficit re litho @ roof (MPa) (ref. 7,5 MPa @1549 mTVNAP)	6,5	6,3	7,9	6,9	7,4	8,1	7,7	9,4	8,0	8,6	6,9
Hmin for salt (m)	19,3	11,0	28,6	19,8	23,2	28,5	26,0	31,2	21,9	23,2	39,7
Hmin for clayey salt (m)	21,9	12,5	32,6	22,5	26,3	32,4	29,5	35,5	24,9	26,3	45,1
2. Pdeficit re litho @ roof (MPa) (ref. 11,0 MPa @1549 mTVNAP)	10,0	9,8	11,4	10,4	10,9	11,6	11,2	12,9	11,5	12,1	10,4
Hmin for salt (m)	25,6	14,7	36,5	26,0	29,9	36,2	33,3	38,7	28,0	29,1	52,0
Hmin for clayey salt (m)	29,0	16,7	41,4	29,4	33,9	41,1	37,8	43,9	31,7	33,1	59,0
3. Pdeficit re litho @ roof (MPa) (ref. 13,5 MPa @1549 mTVNAP)	12,5	12,3	13,9	12,9	13,4	14,1	13,7	15,4	14,0	14,6	12,9
Hmin for salt (m)	30,1	17,4	42,3	30,4	34,8	41,9	38,6	44,2	32,4	33,5	61,0
Hmin for clayey salt (m)	34,0	19,6	47,9	34,5	39,5	47,5	43,8	50,1	36,7	38,0	69,1
Total ZE roof thickness (m)	95	92	104	96	75	106	103	107	111	110	79

Table 9: Minimum roof thickness for stability of each 3b-cavern roof for two rock compositions (salt = halite) and for three pressure regimes (process phases).

In Table 9 the calculated minimally required roof thicknesses are summarized per cavern for the three above pressure regimes and for maximum roof diameters, given in Table 7. The thicknesses have been calculated for an optimistic case of pure halite roof and a most pessimistic case, when the roofs would consist of weaker clayey halite only.

The numerical results of Table 9 clearly show that during all process phases, involving brine pressures significantly below local lithostatic pressure, the Zechstein roofs remain stable. Two additional remarks are functional to this result.

In a recent investigation of the TR-4 cavern roof status a wash-out was detected that has taken away an estimated 0.3% (315 m²) of the total roof area (ref.11). This minor area reduction has no impact on gross roof stability. So, as far as the total roof area is concerned local roof damage around the last cemented casing shoe will have a very limited impact on the overall supporting thickness of the Zechstein roof.

As second remark it is stressed that the safety margins for all roof thicknesses are more than sufficient. Even the caverns with the thinnest roofs and biggest roof spans have enough safety margins. For example, for the most challenging pressure deficit case: 13.5 MPa bleed-off and clayey salt roof, cavern TR-7 has a minimum safety margin of 9.9 m. In fact, this case is theoretical, because the roof of TR-7 predominantly consists of pure halite (69 m, see Table 8), giving a safety margin of 18.0 m. The safety margins for all other cases and all other caverns are obviously far better. Another cavern TR-1 with a relatively thin ZE roof has a minimum margin of 35.5 m (clayey halite). Under normal operational conditions all safety margins are excellent, with the smallest margin in case of TR-7 (margin 39.3 m, required 39.7 m, thus safety margin is $39.3/39.7 = 99\%$).

The next question on roof quality addresses the hydraulic integrity. This aspect is of prime importance after final abandonment of the cavern system, when the brine pressure increases as a result of long-term cavern convergence and the pressure deficit gradually turns into a potential pressure surplus re lithostatic pressure. This item is studied in detail in chapter 6.

6 Cavern system integrity after definite abandonment

After cavern sealing, brine pressure quickly increases to lithostatic values. This chapter presents the results from an investigation into the hydraulic and technical integrity (roof and wellbore tightness) of the cavern system in case of high brine pressures.

Attachment 9 gives for two moments in time a graphic overview of the smallest distances between the upper 3b caverns and the overlying permeable Lower Bunter formation. For all sorts of causes most distances decrease between 2000 and 2015, except for VE-1. In 2005 a re-interpretation of VE-1 logs revealed that the bottom of the Lower Bunter is positioned 11 m shallower than originally determined. Despite this modification the last cemented casing shoe of well VE-1 is still positioned nearest by far to the Lower Bunter. The composition of the locally thin roof of cavern VE-1 is shown in attachment 10. The roof with 21 m thickness only consists of 16 m bedded salt clay, covered by a 5 m thick anhydrite layer. Because of these unfavorable circumstances the integrity analysis in this chapter is focused on the VE-1 3b cavern.

Pressures near VE-1 shoe in abandonment situation (worst case analysis)

It is assumed that instantaneously at the start of the abandonment phase the brine pressure in the cavern system increases to lithostatic values. The medium bottom depth of the system is at 1726 m TV NAP. The average pressure gradient of the enclosed system brine is taken as 0.0135 MPa/m, whereas the lithostatic gradient is 0.022 MPa/m. The salt creep and cavern convergence increase with depth. This implies that in a continuous brine column the brine pressure at shallower depth is controlled by the deeper parts of the system. To date, 3b cavern VE-1 is still isolated from the surrounding caverns. As worst case it is assumed that at the time of final abandonment cavern VE-1 is integral part of the overall hydraulic system and that the VE-1 shoe functions as the system's brine leak-off point. In attachment 11 the VE-1 cavern situation is shown, including the stratigraphy and dimensions most relevant to the hydraulic processes in the abandonment phase. The VE-1 shoe is positioned at a depth of 1365 m TV NAP. The soil surface level is at +2 m NAP.

The pressure $P_{b,roof}$ of the enclosed free brine at the top of the VE-1 cavern tends to a level of circa 3 MPa above local lithostatic pressure $[(1726-1365) \cdot (0.022-0.0135)]$. As shown in the graph of attachment 12 even a small brine overpressure relative to the local lithostatic pressure P_{litho} , denoted as (positive) effective stress σ_{eff} , causes a very significant increase of salt permeability. When the salt becomes more permeable, brine will leak off faster and the brine pressure falls back to lithostatic values.

In practice, the resulting equilibrium involves a permanently enhanced salt permeability at a brine pressure level hardly exceeding local lithostatic pressure. The equilibrium brine pressure at the VE-1 shoe is about 30 MPa. The bottom of the Lower Bunter is at a depth of 1344 m TV NAP. The pores of the Lower Bunter contain salty water with a gradient of about 0.011 MPa/m, giving a pore pressure $P_{hyd, LB}$ at the bottom of circa 14.8 MPa. This means that a fluid pressure difference ΔP of 15.2 MPa exists over a Zechstein roof section of 21 m thick only.

Brine permeation through the VE-1 Zechstein roof

The hydraulic processes are strongly determined by porosity and permeability of the rock materials involved. In Table 10 a summary of literature values for porosity and permeability K is given (refs.12-19).

	Permeability K [m²]	Porosity [%]
Pure halite	$< 10^{-21}$	0.1 . 0.2
Halite inter-bedded with claystone and anhydrite	$2 . 9 \cdot 10^{-19}$	0.2 . 1
Anhydrite	$< 10^{-21}$ (undisturbed) $10^{-16} . 10^{-19}$ (disturbed)	0.5 . 3
Lower Bunter sandstone/ mudstone (clayey and tight)	$10^{-15} . 4 \cdot 10^{-18}$	4 . 10
Main Bunter sandstone	$1 . 7 \cdot 10^{-13}$	12 - 22

Table 10: Permeability and porosity values for five rock types adopted from the literature

The permeation and leak-off pattern around the VE-1 casing shoe is schematically shown in attachment 11. The process is modeled under the following assumptions:

- The permeation process is cone shaped with 45° angle to the vertical
- The tip of the inverted cone is placed 4 m below the casing shoe making the cone height 25 m with an average disc-shaped cone diameter of 25 m.
- The porosities of the clayey salt and anhydrite are both 5%
- The cavern neck section below the cone tip is neglected.

The pore volume of the permeation cone $V_{\text{pore}} = \pi r^2 h = 81.8 \text{ m}^3$. According to the two-branch squeeze model output in Table 5 the base case brine permeation in the first abandonment year amounts to 477 m^3 ($\approx 1.5 \cdot 10^{-5} \text{ m}^3/\text{s}$, 1 year = $31.536 \cdot 10^6 \text{ s}$). This number implies that after two months of cavern abandonment carnallitic brine would start flowing into the Lower Bunter formation.

The fluid pressure decline is 15.2 MPa over a roof trajectory of 21 m only. It seems unlikely that the thin roof can permanently accommodate the intensive permeation flow caused by the large pressure drop.

Hydraulic capacity of the VE-1 cavern roof

The hydraulic capacity of the Zechstein roof has been analyzed by means of Darcy's law for laminar fluid flow. The brine pressure at the top of the VE-1 cavern tends to a level of circa 3 MPa above local lithostatic pressure. According to the data in attachment 12 the permeability of pure salt could probably increase with a factor 10^6 . However, the roof is composed of clayey salt and (disturbed) anhydrite. Combining the permeability data of Table 10 and attachment 12 indicates that a permeability increase by a factor 10^4 to 10^5 is plausible. Furthermore, the cement permeability of the last cemented casing shoe and the cemented casing of well VE-1 is considered identical to the enhanced permeability of the roof rock.

The brine flow through the cavern roof is modeled with Darcy's law as follows:

$$\dot{V} = \frac{K}{\eta} \cdot \frac{A}{\Delta l} \cdot \Delta P$$

Where: \dot{V} = brine flow through VE-1 cavern roof [m^3/s]
 K = enhanced roof permeability $\approx 10^{-16}$ to 10^{-17} m^2 (0.1-0.01 mD)
 η = brine viscosity = $1.2 \cdot 10^{-9} \text{ MPa}\cdot\text{s}$
 A = average area of carnallitic brine permeation $\approx 500 \text{ m}^2$ (disc with 25 m diameter)
 Δl = roof thickness = flow path length = 21 m

^a $P =$ (maximum) difference between cavern roof brine pressure $P_{b,roof}$ and hydrostatic pore pressure $P_{hyd,LB}$ in Lower Bunter ¹ 15.2 MPa.

The calculated Darcy flow varies between $3 - 30 \cdot 10^{-6} \text{ m}^3/\text{s} = 95 - 950 \text{ m}^3/\text{year}$. As the base case model squeeze amounts to 477 m^3 in the first abandonment year, the flow capacity of the roof is potentially outreached. In the no bleed-off case mentioned in chapter 4 the calculated first-year flow is about 31300 m^3 , a value too large by far in view of the permeation capacity of the roof.

If the squeeze model output is the result of an autonomous salt creep process not controlled by physical processes and rock properties elsewhere in the subsurface, the calculated volumes have to be taken for granted, indeed. Then, measures should be taken to reduce the squeeze volumes after abandonment. However, recent references in the literature are that the squeeze process is not a purely stand-alone mechanism. This aspect is further explained in chapter 7.

Prolonged pre-abandonment bleed-off

In view of the above analysis the VE-1 roof integrity should be permanently secured by limiting initial permeation flow to a maximum of circa $100 \text{ m}^3/\text{year}$. This requires an adequate bleed-off period before the cavern field is definitely abandoned. The two-branch squeeze model volume in the first abandonment year is about 2.8% of the remaining free brine volume after the bleeding-off phase (see Table 5). The reduction of the permeation flow to about $100 \text{ m}^3/\text{year}$ requires the free brine volume at the start of the abandonment phase to be restricted to circa 40000 m^3 . This low residual volume is only attainable by introducing a prolonged bleed-off phase with larger sub-lithostatic pressures in the caverns than presented in Table 5.

Provisional calculations using the two-branch squeeze model indicate that a prolonged bleed-off period of 12 years is needed with a permanently increased pressure deficit of 15 MPa at the average shoe depth of 1549 m TV. Then, the remaining free volume at the start of final abandonment is about 44000 m^3 and the first year squeeze volume is about 105 m^3 . In order to achieve a pressure deficit of 15 MPa special measures are needed. The brine to be squeezed out has a specific weight between $1.32 \text{ tons}/\text{m}^3$ (carnallitic brine) and $1.37 \text{ tons}/\text{m}^3$ (bischofitic brine). To obtain a pressure deficit of 15 MPa at a depth of 1549 m TV the fluid gradient must not exceed a value of circa $0.012 \text{ MPa}/\text{m}$, equivalent to a specific fluid weight of $1.2 \text{ tons}/\text{m}^3$. Therefore, the squeezed-out brine should continuously be diluted by water injection via a dilution string installed in the well bore as deep as possible to keep the squeeze process sufficiently going.

The effect of the larger pressure deficit on roof stability has been checked. For the most critical cavern TR-7 a minimum halite roof thickness of 66.7 m is required, which is 5.7 m extra compared to the 13.5 MPa case. A safety margin of 12.3 m remains. For TR-1 the clayey salt minimum roof thickness is 42.9 m, an increase of 3.4 m, with a remaining safety margin of 32.1 m.

In chapter 8 it is explained that, in fact, the prolonged bleed-off case including such high pressure deficits is not necessary in advance of safe cavern field abandonment. The reason for this conclusion lies in a revision of the WEP squeeze model presented next.

7 WEP squeeze model revision

Essentially, the above applied relative squeeze model and the two-branch squeeze model consist of the Norton-Hoff salt creep law. The models have been calibrated based on salt creep and convergence observations from Frisia cavern BAS-1 (ref.2) under stationary operational conditions. Recently, the Frisia salt creep models have been revised (ref.20) for the abandonment case and the immediate cause of it also has an impact on the modeling in this report.

7.1 New permeation concept for sealed brine-filled caverns

Some years ago a new brine permeation model for sealed brine-filled caverns has been developed at the Technical University Clausthal, Germany (refs.21-23) that is based on the LUBBY-2 salt creep law and Darcy type brine flow through porous media. According to this model the continuous creation of secondary porosity in the impermeable salt body significantly delays the progress of the brine infiltration front in the salt. This retarding process also slows down the salt creep and cavern convergence. On a micro scale the formation of new micro migration paths between the salt crystals causes a local and temporary pressure loss in the migrating brine. So, in order to create and keep open salt crystal dislocations through which brine can migrate following Darcy's flow law, energy is needed. On a macro scale this energy consumption is revealed by decreased cavern convergence.

WEP model revision of abandonment conditions

The original WEP squeeze model does not comprise a retarding Darcy flow process. Brine migration and permeation are solely controlled by the cumulative cavern convergence, which is a function of the brine pressure deficit versus lithostatic pressure (split and calculated for 3 model cuts). A more realistic approach is the introduction of an equilibrium pressure for the enclosed cavern brine by equalizing cavern convergence and Darcy controlled brine migration into the salt roof (ref.24).

In fact, the mentioned equilibrium approach has approximately been applied in chapter 6. The calculated Darcy flow varies between 95 - 950 m³/year, based on an increased salt permeability (macro scale approach) as a result of positive effective brine pressure at the roof of the abandoned cavern. The two-branch squeeze model calculates 477 m³ cavern convergence in the first abandonment year. The calculation is based on $p_{eff} = 0$ MPa at the leak-off point (VE-1 shoe) at a depth of 1365 m TV NAP. Then, as earlier shown in chapter 3 the pressure deficit in model cut 2 (bischofitic layer) at a medium depth of 1695 m amounts to 2.84 MPa and in cut 3 (carnallitic layer) at a medium depth of 1582.5 m to 1.91 MPa. This approach is not consistent, because the salt permeability is enhanced for positive p_{eff} at the leak-off point, whereas the squeeze model assumes zero p_{eff} .

7.2 Balanced brine squeeze and migration model

In case of cavern sealing and abandonment the pressure deficits in the WEP salt creep model should be reduced and fine-tuned in order to bring the squeeze volume output in line with the hydraulic capacity of the salt roof for migrating brine. For very small differential pressures the non-linear salt creep component is almost negligible, as shown in attachment 6. The following simplified equilibrium relation [m³/s] has to be solved, with p_{eff} as unknown parameter:

$$K_h / \cdot A \cdot (P + p_{eff}) / I \dot{A}^3 \text{ cuts2\&3 } \{ V_{cav.3} \cdot (P_{cav} - p_{eff}) \cdot M_{salt,aver} \cdot A_2 \cdot e^{-Q/RT} \}$$

Where: K_h = permeability of halite dependent of positive effective stress σ_{eff} [m^2]
 P = difference between lithostatic brine pressure at leak-off point and pore pressure in Lower Bunter, increased with positive σ_{eff} at leak-off point [MPa]
 V_{cav} = free brine volume left in caverns, split in model cut 2 and model cut 3 [m^3]
 P_{cav} = cavern brine pressure deficit re local lithostatic (≈ 0.009 MPa/m), to be reduced with the positive σ_{eff} value at leak-off point [MPa]
 $M_{salt,aver}$ = average salt mobility factor for model cuts 2 and 3, relative to halite
 T = brine temperature
 Q/R = activation energy
 A_2 = linear squeeze model coefficient for halite = $0.161 \cdot 10^{-3}$ /s.MPa
 A_1 , I , see application of Darcy formula in chapter 6.

Permeability K_h as a function of effective brine pressure σ_{eff} at the leak-off point is taken equal to the linear IUB criterion (see attachment 12), but without cut-off at 1 MPa:

$$K_h = 10^{-21} \cdot 10^{3 \cdot \sigma_{eff}} [m^2], \text{ for conditions where } \sigma_{eff} \geq 0 [MPa].$$

In Table 11 the applied parameters for the salt creep model cuts are summarized.

Average model	Depth (m)	P_{cav} (MPa)	V_{cav} . after & no bleed-off (m^3)		$M_{salt,aver}$ (-)	T (K)	Q/R (K)	$A_2 \cdot e^{-Q/RT}$ (1/(s.MPa))
Cut 2	1695	2.84	$0.9 \cdot 10^3$	$1.03 \cdot 10^6$	59	339	6201	$0.183 \cdot 10^{-11}$
Cut 3	1582.5	1.91	$165 \cdot 10^3$	$0.82 \cdot 10^6$	16	335	6201	$0.147 \cdot 10^{-11}$

Table 11: Input parameters for salt creep in model cuts for abandonment phase (base case) and leak-off point at 1365 m TV NAP. $M_{salt,aver}$ is based on the 1-40-160 salt mobility relationship.

After inserting all known parameters pertinent to the bleed-off case the equation to be iteratively solved for σ_{eff} [MPa] is:

$$(15.2 + \sigma_{eff}) \cdot 10^{3(\sigma_{eff}-2)} + 0.6 \sigma_{eff} \dot{\epsilon} - 1.16 = 0, \text{ yielding as result: } \sigma_{eff} = 1.42 \text{ MPa.}$$

For $\sigma_{eff} = 1.42$ MPa the enhanced salt permeability becomes: $K_h = 10^{-16.74} = 1.3 \cdot 10^{-17} m^2$ and Darcy's brine flow through the VE-1 roof under equilibrium conditions is $4.5 \cdot 10^{-6} m^3/s \approx 140 m^3/year$ in the first year of abandonment, assuming immediately lithostatic brine pressures in the caverns. The pressure deficit in cavern model cut 2 is 1.42 MPa and in model cut 3 it is 0.49 MPa only. For these small pressure deficits in the abandonment phase the contribution of the non-linear salt creep component to the brine squeeze is practically negligible.

Purely stand-alone squeeze model not adequate in abandonment phase

The choice made in chapter 6 on expected roof permeability (10^{-16} to $10^{-17} m^2$) very well coincides with the permeability resulting from the above pressure equilibrium approach. The general conclusion from these analyses of the hydraulic capacity of the VE-1 roof is that under abandonment conditions the application of a stand-alone squeeze model leads to unrealistic cavern convergence volumes, such as presented in chapter 4 and Table 5. Therefore, as explained above an appropriate alternative is the application of an equilibrium relation between cavern convergence and hydraulic roof capacity.

Feasibility of no bleed-off case reconsidered

According to the stand-alone two-branch squeeze model the permeation rate in the first year after immediate cavern field abandonment without prior bleeding-off would amount to circa 31000 m³. This number looks quite unrealistic. So, the balanced model relation is also introduced for the no-bleed-off case with input figures taken from Table 11. In 2025 at the start of final abandonment the available free brine volume is 1.85 million m³; split into 1.03 million m³ for model cut 2 and 0.82 million m³ for cut 3. The equation to be solved is:

$$(15.2 + p_{\text{eff}}) \cdot 10^{3(p_{\text{eff}}-2)} + 19.7 p_{\text{eff}} - 53.3 = 0, \text{ yielding } p_{\text{eff}} = 1.97 \text{ MPa.}$$

This solution is remarkable in view of the conventional pressure deficit in cut 3 amounting to 1.91 MPa. If this deficit is reduced by a positive p_{eff} of 1.97 MPa, the brine pressure in cut 3 evolves towards a value slightly exceeding local lithostatic pressure. No cut-3 cavern convergence would occur. Instead, because of the strong squeeze drive originating from the bischofitic cut-2 cavern section brine would start permeating somewhat into the salt formation surrounding the upper 3b cavern section of VE-1.

For $p_{\text{eff}} = 1.97 \text{ MPa}$ the enhanced salt permeability becomes: $K_h = 10^{-15.1} = 7.9 \cdot 10^{-16} \text{ m}^2$ and Darcy's brine flow through the VE-1 roof under equilibrium conditions is $0.27 \cdot 10^{-3} \text{ m}^3/\text{s} \cdot 8600 \text{ m}^3$ in the first year of abandonment. This equilibrium controlled volume is a factor 4 smaller than derived by means of stand-alone squeeze modeling.

In view of the VE-1 Zechstein roof composition, being clayey salt and anhydrite of in total 21 m thick with assumed porosities of 5%, the necessary equilibrium permeability and first year brine flow of 17.2 m³ per m² roof area (1 47 l/day) possibly causes a hydrodynamic overcharge of the roof material. If a fifth of porosity would be available for laminar brine flow, this would provide flow channels of effectively 100 cm² area per m² of permeating roof. This would result in circa 0.47 l/day to flow through only 1 cm² of flow area of many individual micro channels. After a while this can lead to a wearing out of the micro channels and gradual breakthrough of the thin roof. On the other hand, the Lower Bunter formation above the Zechstein roof is a sort of tight mudstone with pertinent properties given in Table 10. Its permeability is in the same range as the calculated pressure-controlled enhanced Zechstein permeabilities. The consequences of the brine migration conditions in the Zechstein roof and Lower Bunter mudstone are further analysed as a coupled system in the next chapter.

8 Migrated brine containment and confinement

After brine has migrated through the Zechstein formation the primary brine containment takes place in the overlying Lower Bunter formation. This formation has a thickness of circa 240 m and consists of somewhat tight mudstone. Based on Table 10 data the following average rock properties are adopted: porosity $\phi_{LB} = 7\%$ and permeability $K_{LB} = 10^{-16} \text{ m}^2$ (0.1 mD). Because of higher specific weight the inflowing carnallitic or bischofitic brine will push up and aside the original salty pore water in the Lower Bunter without turbulence or appreciable blending.

8.1 Integrally coupled balanced brine squeeze and flow process

Darcy's laminar flow law is applied for modeling the hydraulic flushing and pushing aside processes in the Lower Bunter. The brine permeation and intrusion process investigated here is an extreme situation representative of the *no-bleed-off case*. The presumed pore pressure at the bottom of the Lower Bunter formation is $P_{\text{hydro}} = 14.8 \text{ MPa}$ at 1344 m TV, giving a pressure difference of 15.2 MPa relative to the lithostatic brine pressure at the VE-1 leak-off point. Elastic brine expansion due to pressure decline during migration is not considered in below analysis. It is further presumed that the brine intrusion creates a brine-filled truncated cone-shaped Lower Bunter bulk volume with a height h , top radius h and base radius $2h$. The bulk volume of this shape is equal to $V_{\text{LB,Bulk}} = \frac{7}{3} h^3$. The area of the average horizontal cross section of this shape amounts to $A_{\text{LB}} = (1.5h)^2$.

The following equations simultaneously determine the brine squeeze and intrusion process at time t [s] after start of abandonment, with unknown parameters dV_{ZE}/dt , P_{ZE} , l_{LB} and P_{eff} :

- 1) Brine flow through VE-1 Zechstein roof, with P_{eff} -dependent roof permeability:

$$dV_{\text{ZE}}/dt = (10^{-21} \cdot 10^3 \cdot P_{\text{eff}}) / (A_{\text{ZE}} \cdot l_{\text{ZE}}) \cdot P_{\text{ZE}}$$

- 2) Brine flow into Lower Bunter formation:

$$dV_{\text{ZE}}/dt = dV_{\text{LB}}/dt = K_{\text{LB}} / (A_{\text{LB}} \cdot l_{\text{LB}}) \cdot (P_{\text{ZE}} - P_{\text{LB}}), \text{ where } A_{\text{LB}} = (1.5 \cdot l_{\text{LB}})^2$$

- 3) Brine-filled truncated cone in Lower Bunter at time t :

$$V_{\text{LB,bulk}} = (dV_{\text{ZE}}/dt) t / l_{\text{LB}} = 7/3 \cdot h^3, \text{ where } h = l_{\text{LB}}$$

- 4) Pressure equilibrium equation:

$$P_{\text{ZE}} + P_{\text{LB}} = 15.2 + P_{\text{eff}}$$

- 5) Equilibrium equation for cavern convergence in abandonment phase:

$$dV_{\text{ZE}}/dt = 3 \cdot \text{cuts}_{2\&3} \cdot \{V_{\text{cav}} \cdot 3 \cdot (P_{\text{cav}} - P_{\text{eff}}) \cdot M_{\text{salt,aver}} \cdot A_2 \cdot e^{-Q/RT}\}$$

With: dV_{ZE}/dt = brine flow from converging cavern into Lower Bunter [m^3/s]

P_{ZE} = pressure loss in brine while flowing through VE-1 Zechstein roof [MPa]

$l_{\text{LB}} = h$ = column height of brine migrated into Lower Bunter at time t [m]

P_{LB} = pressure loss of brine migrating into the Lower Bunter formation [MPa]

P_{eff} = effective brine pressure at VE-1 leak-off point [MPa] (see chapter 7),

with all other parameters specified before in chapters 6 and 7.

At the start of abandonment the free brine volume in the no-bleed-off case is 1.85 million m³. The above five equations have been solved for the brine migration situation after one year of cavern field abandonment. Inserting all known values and solving for parameter p_{eff} yields:

$$(15.2 + p_{eff} \cdot 43.106 \cdot 0.39 p_{eff}^{2/3}) \cdot 10^{3(p_{eff}-2)} + 19.7 p_{eff} \cdot 53.4 = 0.$$

Iteratively solving the equation leads to a zero-sum result for $p_{eff} = 2.20$ MPa.

The calculated p_{eff} of 2.20 MPa seems physically unlikely in view of the conventional pressure deficits of 2.84 MPa in cut 2 and 1.91 MPa in cut 3. The strong squeeze drive from the bischofitic cut-2 cavern section would start pressing brine not only into the salt roof around the shoe of VE-1, but also in the complete upper 3b cavern section of VE-1. Using $p_{eff} = 2.20$ MPa the following values are calculated for the other unknown parameters: $K_h = 4 \cdot 10^{-15}$ m²; $dV_{ZE}/dt = 0.202 \cdot 10^{-3}$ m³/s \approx 6400 m³/year; $h = 23.2$ m; $P_{ZE} = 2.56$ MPa; $P_{LB} = 14.8$ MPa; $A_{LB} = 3800$ m²; $V_{LB,Bulk} = 91.5 \cdot 10^3$ m³. Particularly, the hydraulic characteristics of brine migration through the Zechstein roof, namely a salt permeability even larger than the Lower Bunter permeability and the unusually small pressure decline in the salt roof seem unrealistic.

8.2 New coupled balanced model for strong squeeze drive

The solution of the above set of equations suggests that the permeation area has to be far larger than the small brine leakage point and permeation pattern with respect to cavern VE-1, shown in the figure of attachment 11. This aspect is further investigated in this section, again for the conservative *no bleed-off case*.

Integral VE-2 leak-off roof instead of VE-1 leak-off point only

The cross section in attachment 13 presents a true-scale illustration of the position of the shallowest 3b caverns in their stratigraphic setting. To date, well VE-1 has no lower 1b cavern and the 3b upper cavern is hydraulically isolated from the other caverns in the field. Also, to date, the lower 1b caverns of wells VE-2 and VE-3 (not depicted) are mutually connected, but they are still isolated from the 1b lower caverns of VE-4 and the TR-wells. So, in that sense attachment 13 actually depicts a conservative situation in anticipation of possible future connections between the 1b caverns of VE-2 and VE-3 with those of VE-4 and TR-7 (so called 1b field labyrinth). The probability of a future direct connection between the upper 3b cavern of VE-1 and the rest of the field cannot completely be excluded, but is deemed low. This low expectation is based on the facts that Nedmag has no further plans to actively produce salts from the 2b/3b carnallite layers and that well VE-1 is definitely inactivated because of its sensitive shallow casing shoe.

In the following analysis it is assumed that the *integral* roof area of the 3b-cavern of well VE-2, containing the shallowest free brine volume in the total field system, is functioning as flow window for migrating brine. As specified in Table 9, the VE-2 Zechstein roof is represented by a circular area with a maximum diameter of 122 m and an average thickness of 92 m. Thus, the new Zechstein permeation area A is about 11700 m². The migration path to the overlying Lower Bunter formation has an average length $l = 92$ m. Furthermore, it is presumed that the brine migration in the roof deviates under a widening angle of 45°. This process creates at the bottom of the Lower Bunter a soaked region with a base radius $R = 153$ m ($122/2 + 92$) and an area $A_{LB} = 73500$ m², out of which brine migrates into the Lower Bunter.

Presumably, in the Lower Bunter a brine-filled truncated cone-shaped bulk volume evolves with base radius $R = 153$ m, height h and upper radius $r = R - h$. The truncated cone volume is equal to: $V_{LB.Bulk} = h(3.153^2 - 3.153h + h^2)$.

The bottom of the Lower Bunter formation above cavern VE-2 is situated at an average depth of 1322 mTV. The hydrostatic pore pressure is 14.5 MPa (gradient 0.011 MPa/m). The roof of the VE-2 3b-cavern is situated at an average depth of 1414 m TV. The conventional local lithostatic brine pressure at the VE-2 roof is 31.1 MPa. Thus, the pressure difference between cavern brine and Lower Bunter pore pressure is 16.6 MPa. In the abandonment situation this value is enlarged by the positive p_{eff} . For a leak-off depth of 1414 m TV the pressure deficit in model cut 3 amounts to 1.48 MPa [$0.0088 \cdot (1582.5 - 1414)$] and in model cut 2 to 2.41 MPa [$1.48 + 0.0083 \cdot (1695 - 1582.5)$].

For the integral VE-2 leak-off roof case a new set of five equations in line with those of section 8.1 is obtained. Apart from the above presented modifications in dimensions (A , A_{LB} , l) and pressure differences (ΔP , ΔP_{cav}) the other parameters are kept equal to those of the former set. The new set of equations can be relatively easily solved for parameter p_{eff} by simplifying the above $V_{LB.Bulk}$ formula into $V_{LB.Bulk} \approx h \cdot 3.153^2$. For values $h < 5$ m, the resulting volume error remains below 3%. The following intrinsic relation for p_{eff} is derived:

$$(15.8 + 1.69 p_{eff} - 0.15 p_{eff}^2) \cdot 10^3 (p_{eff} - 2) + 3.68 p_{eff} - 8.38 = 0.$$

Iteratively solving the equation leads to the zero-sum result $p_{eff} = 1.69$ MPa.

For $p_{eff} = 1.69$ MPa the enhanced salt permeability becomes: $K_h = 1.17 \cdot 10^{-16}$ m² and Darcy's brine flow through the VE-2 3b-roof under equilibrium conditions is $0.23 \cdot 10^{-3}$ m³/s \approx 7250 m³ in the first year of abandonment assuming lithostatic brine pressures in the caverns. Clearly, these hydraulic figures imply that the salt is not a tight rock anymore under the given circumstances. The flow of 7250 m³ occurs through a roof area of 11700 m², giving 0.62 m³ flow per m² per year at maximum (\approx 1.7 l/day). This flow capacity demand looks acceptable, when taking into account an increased secondary salt porosity of circa 1% (ref.23).

For $p_{eff} = 1.69$ MPa the pressure deficit in VE-2 cavern model cut 2 (1b section) is 0.72 MPa, but in model cut 3 (3b/2b section) a surplus of 0.21 MPa is present. Likely, this surplus will press some brine volume laterally into the salt formation surrounding the upper 3b cavern of VE-2. The brine pressure loss ΔP_{ZE} during brine flowing through the VE-2 Zechstein roof is 18.2 MPa (\approx 2 bar/m roof). The brine pressure loss ΔP_{LB} in the Lower Bunter is 0.1 MPa only. This loss value equally defines the overpressure with which the migrating brine enters the bottom of the Lower Bunter formation. The first year intrusion height h of the escaping brine into the Lower Bunter formation is 1.4 m.

8.3 Extended balanced two-branch squeeze model

In order to enable meaningful application of the two-branch squeeze model, as introduced in chapter 4, under typical abandonment conditions the model has been extended by inserting parameter p_{eff} . In line with equation 5 of paragraph 8.1, the term ΔP in the model has been replaced by $(\Delta P - p_{eff})$. The modified two-branch squeeze model is called balanced model.

Solving the coupled five-equations-model of paragraph 8.2 has yielded $p_{eff} = 1.69$ MPa and a first year brine flow through the VE-2 roof of circa 7250 m³. The balanced two-branch squeeze model has been matched to these data. Then, the matched balanced model provides simple calculation of squeeze volumes 100 years after cavern sealing and abandonment.

According to the original two-branch squeeze model, applied in the no bleed-off case, the abandonment phase starts in 2025 after $9.43 \cdot 10^6 \text{ m}^3$ squeeze and with a remaining free brine volume of $1.85 \cdot 10^6 \text{ m}^3$. The first abandonment year squeeze volume is about 31300 m^3 . After 100 years of cavern sealing the cumulative squeeze volume is $1.17 \cdot 10^6 \text{ m}^3$, bringing total squeeze to a cumulative volume of $10.60 \cdot 10^6 \text{ m}^3$ with resulting 63.6 cm land subsidence.

The balanced two-branch squeeze model delivers quite different results for the no bleed-off case. For $p_{\text{eff}} = 1.69 \text{ MPa}$ the brine production can continue until 2027. At the start of final cavern sealing and abandonment the total squeeze volume is $10.13 \cdot 10^6 \text{ m}^3$ and the remaining free brine volume is $1.64 \cdot 10^6 \text{ m}^3$. The squeeze in the first abandonment year is circa 7150 m^3 and after 100 years the cumulative squeeze is $0.41 \cdot 10^6 \text{ m}^3$, bringing total squeeze to a cumulative volume of $10.54 \cdot 10^6 \text{ m}^3$ and resulting land subsidence of 63.3 cm.

8.4 Lower Bunter containment analysis

According to the integrally coupled balanced modeling of section 8.2 the Lower Bunter has to accommodate circa 7250 m^3 of migrated brine during the first abandonment year, in the extreme case that the pre-abandonment bleed-off phase is completely left out. The brine enters the bottom of the Lower Bunter formation with circa 0.1 MPa overpressure, relative to the original hydrostatic pore pressure. The imposed overpressure in the Lower Bunter mudstone is by far too low to cause any sort of hydraulic rock fracturing, as shown below.

Stress field analysis in Lower Bunter

Mudstone is not very stiff rock. The Poisson ratio is about 0.275, thus $\nu_{\text{h,eff}} \approx 0.38 \nu_{\text{v,eff}}$. The mudstone is in contact with the Zechstein formation in which isotropic stress conditions prevail ($\sigma_{\text{h,eff}} \approx \sigma_{\text{v,eff}}$). When over-pressured brine is entering the mudstone in the horizontal plane, stress conditions are comparable to those in a fluid-filled horizontal borehole. In gravitation controlled stress fields even minor overpressures P in the borehole relative to the local hydrostatic pressure may cause vertical tension fractures in the rock. Critical overpressure is calculated as follows: $P_{\text{crit}} = 3 \nu_{\text{h,eff}} \cdot \nu_{\text{v,eff}}$ (ref.25). Inserting $\nu_{\text{h,eff}} \approx 0.38 \nu_{\text{v,eff}}$ results into $P_{\text{crit}} \approx 0.14 \nu_{\text{v,eff}}$. At the bottom depth of 1322 m TV it holds $\nu_{\text{v,eff}} = P_{\text{lithost}} \cdot P_{\text{pore}} = 1322 \times 0.011 = 14.5 \text{ MPa}$ and $P_{\text{crit}} \approx 2 \text{ MPa}$. This P_{crit} is a conservative value, in which the cohesion of mudstone is neglected. The analysis shows that rock fracturing as a result of brine intrusion is extremely unlikely.

Furthermore, at the very bottom of the mudstone the stress field is influenced by the isotropic stress conditions in the Zechstein formation. This means that $\nu_{\text{h,eff}}$ tends towards $\nu_{\text{v,eff}}$ and that P_{crit} tends towards values far larger than 2 MPa. These conditions make Lower Bunter fracturing by brine intrusion practically impossible.

Pore-fluid pushing-aside process in Lower Bunter without fracturing

The following properties apply to the modeling of the brine intrusion and fading-away process (no-bleed-off case) in the Lower Bunter mudstone:

- ~ In-situ brine compressibility $\beta_{\text{brine}} = 2.7 \cdot 10^{-4}/\text{MPa}$ (ref.12)
- ~ Compressibility of Lower Bunter rock matrix $\beta_{\text{rock}} = 1.1 \cdot 10^{-4}/\text{MPa}$ (refs.26, 27)
- ~ Bulk compressibility Lower Bunter $\beta_{\text{LB}} = 1.2 \cdot 10^{-4}/\text{MPa}$ (for $\beta_{\text{LB}} = 7\%$).

During the first abandonment year circa 7250 m^3 pore fluid is pushed aside by the intruding brine from the Zechstein formation. This pushed away volume will gradually spread over a huge rock bulk volume. Assume, for example, that in one year time the original pore fluid has

spread itself in a storage cylinder with a height of 240 m (= Lower Bunter thickness) and radius of 1 km. The bulk volume of this cylinder is $V_{\text{bulk}} = 754 \cdot 10^6 \text{ m}^3$. The local net pressure increase in this zone of the Lower Bunter formation is $P_{\text{cyl}} = 7250 / (V_{\text{LB}} \cdot V_{\text{bulk}})^{1/3} = 0.08 \text{ MPa}$. This pressure increase is very moderate compared to P_{crit} of 2 MPa and will not affect the local rock circumstances.

Brine containment capacity of Lower Bunter formation

On geological time scale the Lower Bunter has to accommodate $1.64 \cdot 10^6 \text{ m}^3$ of invaded brine. This requires $23.4 \cdot 10^6 \text{ m}^3$ of gross rock storage volume for $V_{\text{LB}} = 7\%$. As it is expected that the final pressure increase in the storage cylinder will stabilize below 0.1 MPa the total volume involved is $1.37 \cdot 10^{11} \text{ m}^3$ [$1.85 \cdot 10^6 / (1.2 \cdot 10^{-4} \cdot 0.1)$]. For an average Lower Bunter thickness of 240 m the radius of the cylinder is 13.5 km. This radius looks feasible in a geological and stratigraphic sense.

8.5 Brine migration confinement by Solling claystone

The Solling claystone overlying the Lower Bunter mudstone is circa 120 m thick. Specific local characteristics of the Solling claystone are not available. General literature data for claystone (refs.28-30) are the following: $K_{\text{clst}} = 10^{-21} \cdot 10^{-17} \text{ m}^2$ and $\alpha_{\text{clst}} = 1 \cdot 10\%$. A general relationship between K and α for shales is the following (ref.13): $K = 0.1 \cdot \alpha^{2.26} + (10 \cdot \alpha)^{10}$ [10^{-18} m^2], with α as fraction. Assume $\alpha_{\text{Soll}} = 0.05$ (5%), then $K_{\text{Soll}} = 0.66 \cdot 10^{-20}$, which value represents a very tight (impermeable) claystone.

However, the Solling claystone is not instrumental or needed as confinement barrier in view of the above analysis results:

- The brine containment capacity of the Lower Bunter mudstone is huge and absolutely sufficient to store all brine escaping from the Zechstein cavern field.
- Short term pore pressure increase amounts to circa 0.1 MPa with a tendency to decrease to even smaller values on the long term.
- The carnallitic and bischofitic brine intruding into the Lower Bunter mudstone is heavier than the original pore fluid and will, therefore, tend to move along and stay at the bottom region of the containment mudstone.

9 Sensitivity analysis

In the previous chapters many models, input and control parameters and assumptions have been introduced and applied. In this chapter the related uncertainties and likelihoods of these elements are considered in some detail.

Generally, two types of uncertainties are involved, namely uncertainties of a stochastic origin (randomness of phenomenon) and uncertainties of an epistemic origin (knowledge related). Stochastic uncertainties are inherent to the typical characteristics of the item under consideration and can usually not be reduced, apart from measurement noise that can be reduced by introducing longer observation periods. In this study most essential uncertainties appear to be related to a present lack of sufficient knowledge on many aspects. The positive message of this conclusion is that future knowledge will diminish the actual uncertainties.

First, an inventory of epistemic uncertainties is made by summarizing the assumptions underlying many of the modeling concepts presented in this study. Then, the same is done for the stochastic uncertainties (spread) in applied input data. Sometimes, the uncertainty in a parameter is a mixture of both epistemic and stochastic origins. Then, the item is assigned to the inventory to which it predominantly belongs. Using these inventories a concise sensitivity analysis is performed to get an impression of the likelihood and reliability of the results achieved.

9.1 Inventory of epistemic uncertainties

Assumptions

The following assumptions have been made as bases for this study:

- Coefficient A_1 of the two-branch squeeze model can be derived from Frisia reference data for non-linear halite creep under stationary conditions.
- For convenient modeling purposes (non)-linear creep of other salt types than halite can be described by just one multiplication factor M_{salt} relative to the creep properties of halite.
- Coefficient A_2 (for halite) of the two-branch model can be derived from uniaxial creep data for bischofite, using a reduction factor of $1/M_{\text{bischofite}}$.
- In all salt layers of the Nedmag mine (Zechstein-III) the standard bulking factor for inert rock and precipitated salts is 1.10 (adopted from approved Winningsplan 2013).
- The actually dissolved salt volumes per cavern and per model cut are unknown; therefore, starting from January 2012 equal free brine volumes are presumed per cut for all caverns, namely cut 1: 10800 m³, cut 2: 145883 m³ and cut 3: 120445 m³.
- After the sealing of all caverns in the brine field, the pressure of the enclosed brine instantaneously raises to local lithostatic values.
- After final cavern sealing the system's shallowest casing shoe (VE-1 @ 1363 m TV) will form the brine leak-off point, which is rather theoretical in view of its isolated position.
- Pressure gradients applied are: ${}^a P_{\text{lithostatic}} = 0.22 \text{ bar/m}$, ${}^a P_{\text{carnal-brine}} = 0.132 \text{ bar/m}$ and ${}^a P_{\text{bischof-brine}} = 0.137 \text{ bar/m}$.
- For roof stability calculations rockmechanical properties derived for halite and salty claystone in the Akzo Hengelo cavern field can be applied.
- The 3b cavern roof spans are conservatively determined by assuming that water injected in the 2b and 3b sections has solely dissolved carnallite in the 3b section.
- The following Lower Bunter properties are assumed (based on literature value ranges): $= 7\%$, $K_{\text{LB}} = 10^{-16} \text{ m}^2$ and pore fluid gradient ${}^a P_{\text{pore-fl}} = 0.11 \text{ bar/m}$ (150 g/l NaCl).
- In the Lower Bunter pores no blending of migrating carnallitic/bischofitic brine with the original pore fluid will occur. It is a gravitational pushing-aside process.

- The brine permeation pattern in the VE-1 roof is inverse-cone-shaped with 45° angle to the vertical and the local roof porosity $\rho_{roof} = 5\%$ (with 1% effective laminar-flow porosity).
- The brine migration pattern in the Lower Bunter is described by a truncated cone.
- Presumably, the integral roof area of the shallow 3b cavern of VE-2 is more likely the system's leak-off point than the shoe region of the isolated 3b cavern of VE-1.
- The pushed-aside pore fluid spreads over the Lower Bunter formation according to a storage cylinder shape with fixed height (240 m) and growing radius in time.

9.2 Inventory of stochastic uncertainties

Most stochastic uncertainties are related to the applied BDS input data and to Gamma ray/ Density logging data. The following list is applicable:

- In order to get overall coincidence between BDS squeeze volumes and the WEP bulked volume model, correction factors have been introduced, varying between -2% and +2%, with average factor zero.
- The activation energy Q of bischofite, having an average value of circa 10 kcal /mol, shows a large spread of 4.9 kcal /mol (\pm). This spread propagates into the activation energy Q/R.
- In order to shift the reference date for squeeze volume calculations from originally July 1993 back to the start of Nedmag salt mining in 1972 the Winningsplan 2013 specifies an additional squeeze volume of 0.5 million m³, based on sub-lithostatic mining conditions. Although not specified, the randomness in this squeeze figure must be significant, with a skewed spread towards lower values.
- The depth of rock layers and the thickness of layers have a spread of circa 1m (\pm).
- The ore concentrations have a spread of circa 5% by volume (\pm).
- Land subsidence as a function of brine squeeze volume amounts to about 6 cm per million m³. This number has a stochastic component, originating from the measurement uncertainty in the levelling surveys ($\pm 1 - 1.5$ cm), and a systematic component, presented in the Winningsplan 2013. The systematic component implies that with increasing total cavern squeeze the amount of subsidence per million m³ decreases. The applied figure of 6 cm applies to the situation of 10 million m³ of cumulative squeeze volume.

9.3 Likelihood and reliability of results obtained

The following aspects will be further analyzed in view of the above presented epistemic and stochastic uncertainties:

1. Salt mobility ratios.
2. Impact of bulking factor on remaining free brine volume.
3. Roof stability during all mining phases.
4. Pre-abandonment bleed-off option.
5. Most critical part of cavern system in view of sealing and abandonment.

Ad 1) Salt mobility ratios

The commonly applied relative salt mobility figures of pure carnallite (=40) and bischofite (=160) are the result of an iteratively optimized best match between BDS-prescribed squeeze volumes and the two-branch squeeze model output during the production period 2012-2026. The model discriminates between squeeze volumes from three cuts, with initial free volumes taken identical for all caverns, but positioned at different depths. The caverns have varying ore compositions specific to each cavern layer. Based on the relative mobility of pure carnallite and bischofite relative to halite, a weighted average mobility figure is determined for each separate cavern cut in order to calculate the squeeze volume. Two control parameters

are essential to the squeeze process during the production period, i.e. the reference pressure deficit $P_{def} = 67.5$ bars at 1463 m TV and the salt activation energy $Q/R = 6201$ K.

It is expected that because of the randomness of deviations in parameters like depth, layer thickness and ore composition, these deviations do not influence the salt mobility values. This also holds for the pragmatic choice of applying free brine starting volumes being identical per well for corresponding model cuts. This choice spreads the squeeze potential as evenly as possible over the salt production activities.

Control parameter P_{def}

The value P_{def} has a very significant impact on the necessary salt mobility ϕ and the linear model coefficient A_2 in order to obtain a satisfactory match between BDS squeeze volumes and the two-branch squeeze volume output. Table 12 shows some typical matching results. The deviations between BDS squeeze volumes and two-branch model squeeze volumes are smaller than 15%.

P_{def} (bar)	$M_{bischofite}$	$M_{carnallite}$	A_2 (1/day.MPa)	$M_{bischofite}/M_{carnallite}$
62.5	210	41	9.3	5.1
67.5	155	38	12.5	4.1
72.5	110	35	17.7	3.3

Table 12: Impact of BDS pressure deficit (at TR-7 shoe) on optimized parameters of two-branch squeeze model.

The pressure deficits P_{def} are held constant during the whole calibration period 2012-2026. This explains the somewhat different M - and A_2 -values in comparison with the Chapter 4 figures. The ratio between bischofite and carnallite mobility ϕ decreases for larger P_{def} , mainly because of lower bischofite mobility ϕ yielding a best match. Apparently, this trend represents the more squeezable character of bischofite salt relative to carnallite.

Control parameter Q/R

The so far presented squeeze modeling applies an identical activation energy $Q/R = 6201$ K for all types of salt. This choice makes it necessary to express differences in creep behavior by means of varying salt mobility factors in the two-branch squeeze model.

However, the specific heat of the various salts is not identical. For example, the specific heat of bischofite is lower than for halite and may vary between limit values of circa 5 and 15 kcal/mol. These limits translate into a range of bischofite activation energies Q/R between 2500 and 7400 K.

Consequently, the impact of varying activation energy values is investigated. In the two-branch squeeze model all salt mobility factors have systematically been set to unity. Then, the different squeeze properties of the various salts are represented by specific Q/R values. Per cavern and per model cut weighted Q/R values are determined on the basis of the local salt compositions.

In order to get a best match with BDS controlled free brine and squeeze volumes the Q/R values have been varied for bischofite, carnallite and halite. The same boundary conditions as pertinent to the Table 12 cases have been used. The modeling results are summarized in Table 13. The deviations between BDS squeeze volumes and two-branch model squeeze volumes are smaller than 5% in the period 2012-2023. After 2023 the deviations increase to values up to 10%.

P_{def} (bar)	A_2 (1/day.MPa)	Q/R_{halite} (K)	$Q/R_{carnallite}$ (K)	$Q/R_{bischofite}$ (K)
62.5	9.3	6025	4600	3100
67.5	12.5	6100	4700	3200
72.5	17.7	6150	4775	3350

Table 13: Impact of BDS pressure deficit (at TR-7 shoe) on optimized Q/R parameters of two-branch squeeze model, with all salt mobility factors M_{salt} kept equal to 1.

The general impression from comparing the results of Tables 12 and 13 is that the two-branch squeeze modeling for different boundary conditions is more stable when using activation energy Q/R as salt squeeze attributes than representing varying salt squeeze properties by multiplication factors M. On the other hand, it is difficult to corroborate the representativeness of the calibrated Q/R values given in Table 13, because of lack of experimental creep data from pure carnallite and bischofite samples. In a recent investigation (ref.40) high purity bischofite samples from well TR-9 have been investigated at a constant temperature of 70 °C, while discarding the temperature dependent term $e^{-Q/RT}$. So, no information on activation energy Q/R has become available from these experiments.

Ad 2) Impact of bulking factor and fixed pressure deficit on free brine volume

WEP modeling data shown in Table 5 indicate that the bulking factor is a decisive parameter for determining the year in which to end active leaching and for the volume of freely movable brine left in the cavern system at the start of the pre-abandonment bleed-off procedure. The data in Table 5 have been obtained by varying the yearly sub-lithostatic pressures according to Table 4 in order to get compliance with BDS cavern convergence volumes.

In reality, during the mining operations a constant pressure deficit of 67.5 bars at TR-7 shoe depth (1480 m TV NAP) is commonly applied. Fine-tuned pressure optimization will not take place, since it is unknown so far which specific bulking factor is most representative for the mine. Therefore, the bulking factor is not a practical parameter for controlling operational pressures in the production phase.

Additionally, modeling until the moment of cavern sealing has been performed using a fixed pressure deficit of 67.5 bars. Table 14 summarizes new results from a sensitivity analysis for bulking factors ranging from 1.08 to 1.12.

Bulking factor	Start year bleed off	Total squeeze at start bleed off (Mm ³)	Free brine at start bleed off (Mm ³)	Total squeeze after 10 years bleed off (Mm ³)	Remaining free brine (Mm ³)
1.08	2018	7.51	3.16	10.43	0.24
1.09	2019	7.68	2.78	10.24	0.22
1.10	2022	8.41	2.16	10.38	0.18
1.11	2028	9.07	1.22	10.15	0.14
1.12	2032	8.57	0.84	9.29	0.12

Table 14: Start year of bleed off phase and free brine volume left after 10 years bleeding off as a function of the bulking factor of insoluble materials. A constant pressure deficit of 67.5 bars is applied during the production phase. Mm³ means million m³.

Clearly, for bulking factors below 1.12 the impact on year of production end (= start year bleed off) is very significant, if total potential squeeze volume should be limited to about $10.5 \cdot 10^6$ m³.

For a bulking factor of 1.12 (or larger) the totally created free brine volume in the cavern system is too little ($9.4 \cdot 10^6 \text{ m}^3$) to produce a cumulative squeeze volume exceeding the limit. The land subsidence limit of 65 cm will *never* be reached in that case.

In view of the apparent very critical sensitivity of free brine volumes for bulking factors a separate Chapter 10 is dedicated to an assessment of realistic bulking factors from a representative literature survey.

Ad 3) Roof stability during all mining phases

In this section the stability of roof spans is investigated for the absolute worst case under all mining circumstances. The roof spans are maximal in the following situation:

- all 2b-3b injection water has only dissolved carnallite in the 3b section,
- the 3b section contains 5 vol.% less carnallite than the average value,
- the 3b section is 1 m thinner than the average.

In Table 15 the resulting worst case roof spans are summarized for all caverns involved. The worst case values are also graphically shown in Attachment 8, relative to the regular minimum and maximum values presented in Chapter 5.

Cavern	Maximum vol. dissolved 3b carnallite (m ³)	Minimum. carnallite content (vol.%)	Maximum volume 3b affected (m ³)	Minimum 3b layer thickness (m)	Maximum 3b roof area (m ²)	Worst case roof diameter (m)
VE-1	245415	42	584321	14	41737	231
VE-2	158493	40	396232	29	13663	132
VE-3	244686	35	699103	8	87388	334
VE-4	214391	45	476424	11	43311	235
TR-1	251144	40	627860	11	57078	270
TR-2	257546	45	572324	7	81761	323
TR-3	380115	56	678777	10	67878	294
TR-4	292100	45	649111	7	92730	344
TR-5	223161	51	437571	9	48619	249
TR-6	190085	51	372716	7	53245	260
TR-7	920255	57	1614482	11	146771	432

Table 15: Input data for determination of 3b section worst case (maximum) roof span.

In Table 16 calculated minimum roof thicknesses for roof stability are given for pressure deficits under conditions of normal production and maximum pre-abandonment bleed-off. In all cases enough roof thickness is available to guarantee roof stability, based on the applied rock mechanical properties for halite ($C = 3.3 \text{ MPa}$, $\phi = 33^\circ$) and for clayey halite ($C = 3.5 \text{ MPa}$, $\phi = 26^\circ$).

In a personal communication with D.Brückner, IfG, Leipzig (SMRI, September 2014), it was mentioned that IfG used to apply the following rockmechanical properties for cavern-stability analyses in bedded rock salts: halite $C = 8 \text{ MPa}$, $\phi = 28^\circ$ and *claystone* $C = 2.8 \text{ MPa}$, $\phi = 21^\circ$. In Table 17 new calculation results are shown for the IfG rock properties. For salt as roof material the differences in required thicknesses between Tables 16 and 17 are hardly noticeable. Remarkably enough, in case of pure claystone roof material (not the case with Nedmag) all roofs would still be sufficiently thick for rock mechanical stability.

Minimum thickness Hmin for cavern roof stability	VE-1	VE-2	VE-3	VE-4	TR-1	TR-2	TR-3	TR-4	TR-5	TR-6	TR-7
Worst case roof diameter 3b cav.(m)	231	132	334	235	270	323	294	344	249	260	432
1. Pdeficit re litho @ roof (MPa) (ref. 7,5 MPa @ 1549 mTVNAP)	6,5	6,3	7,9	6,9	7,4	8,1	7,7	9,4	8,0	8,6	6,9
Hmin for salt (m)	21,1	11,9	32,5	21,9	25,7	31,6	28,4	35,2	24,3	26,0	40,2
Hmin for clayey salt (m)	24,0	13,6	36,9	24,9	29,2	35,9	32,2	40,0	27,6	29,6	45,7
2. Pdeficit re litho @ roof (MPa) (ref. 13,5 MPa @ 1549 mTVNAP)	12,5	12,3	13,9	12,9	13,4	14,1	13,7	15,4	14,0	14,6	12,9
Hmin for salt (m)	32,9	18,8	48,0	33,6	38,7	46,5	42,2	49,8	35,8	37,6	61,8
Hmin for clayey salt (m)	37,2	21,2	54,4	38,0	43,8	52,6	47,8	56,5	40,6	42,6	69,9
Total ZE roof thickness (m)	95	92	104	96	75	106	103	107	111	110	79

Table 16: Minimally required roof thicknesses for worst case roof spans in case of (1) regular operations and (2) bleed-off phase with high pressure deficit.

Minimum thickness Hmin for cavern roof stability	VE-1	VE-2	VE-3	VE-4	TR-1	TR-2	TR-3	TR-4	TR-5	TR-6	TR-7
Worst case roof diameter 3b cav.(m)	231	132	334	235	270	323	294	344	249	260	432
1. Pdeficit re litho @ roof (MPa) (ref. 7,5 MPa @ 1549 mTVNAP)	6,5	6,3	7,9	6,9	7,4	8,1	7,7	9,4	8,0	8,6	6,9
Hmin for salt (m)	21,2	12,0	32,9	22,1	26,0	32,0	28,7	35,8	24,6	26,4	40,5
Hmin for claystone (m)	26,6	15,0	41,0	27,6	32,4	39,9	35,8	44,3	30,6	32,8	50,7
2. Pdeficit re litho @ roof (MPa) (ref. 13,5 MPa @ 1549 mTVNAP)	12,5	12,3	13,9	12,9	13,4	14,1	13,7	15,4	14,0	14,6	12,9
Hmin for salt (m)	32,3	18,4	47,6	33,1	38,3	46,2	41,9	49,8	35,5	37,5	60,9
Hmin for claystone (m)	41,4	23,6	60,4	42,3	48,7	58,5	53,2	62,7	45,1	47,3	77,8
Total ZE roof thickness (m)	95	92	104	96	75	106	103	107	111	110	79

Table 17: Minimally required roof thicknesses using an alternative set of rock properties for pure salt and claystone. N.B. In the Nedmag mine claystone is not present as supporting roof element.

No creation of sink holes above Nedmag caverns

In practice, sinkholes above caverns only occur in case of shallow caverns, which are usually overlain by rather unconsolidated overburden material with a low bulking factor. This is very much different from the Nedmag caverns where the overburden is not only very thick but also consists of dense consolidated material with appreciable bulking factors. The overburden stratigraphy is shown in attachments 1, 11 and 13.

In the merely theoretical circumstance of roof degradation and upward migration of a Nedmag cavern the process will soon be choked by the bulking of the degraded roof material. Thus, migration of a cavern through more than 1400 m overburden is considered impossible.

Ad 4) Optional pre-abandonment bleed-off

In the approved ~~Winningsplan~~ 2013 the pre-abandonment bleed-off phase has been presented as an integral part of the mining plan. This study has shown that a bleed-off phase should rather be considered as an option, not as a necessity for save cavern sealing and abandonment.

The no bleed-off case and its possible consequences have been amply investigated in this study. The main findings are as follows:

- Application of a stand-alone squeeze model is not justified in the abandonment phase of a sealed cavern. Such modeling leads to brine migration volumes into the cavern roof being by far too large to be physically realistic.
- An appropriate equilibrium relation between cavern convergence and hydraulic roof capacity must be applied. As first approach a balanced model has been introduced that simultaneously controls the cavern salt creep and the salt roof permeability by means of a balancing effective stress relative to the local lithostatic pressure at the interface between free cavern brine and cavern salt roof.
- The balanced model starts with an enclosed free brine volume of $1.85 \cdot 10^6 \text{ m}^3$ at the end of the production period in December 2024. The modeling results in an equilibrium positive stress of nearly 2 MPa re local lithostatic pressure and brine squeeze volume of circa 8600 m^3 during the first year 2025 of definite field abandonment.
- If the yearly brine squeeze volumes would have to leave to cavern system through the small VE-1 Zechstein casing shoe area only (roof thickness 21 m, permeation area 500 m^2) this may lead to gradual wearing out and breakthrough of the roof. The question about which part of the roof system is most sensitive and decisive in the abandonment phase is further discussed in item 5 of this chapter.
- After brine migration through the Zechstein roof primary brine containment takes place in the overlying Lower Bunter mudstone, which according to literature is a rather tight rock. Therefore, in this study an integrally coupled balanced brine squeeze and permeation model has been developed that consists of five equations, simultaneously describing the rock mechanical and hydraulic processes involved.
- The integrally coupled model demonstrates that it is implausible that for strong squeeze drives, like in a no bleed-off case, brine permeation would be restricted to the VE-1 casing shoe area alone. Likely, the permeation area is far larger and comprises at least the complete VE-2 roof area of about 11700 m^2 and with Zechstein roof thickness of 92 m. The coupled model calculates a brine squeeze volume of circa 7250 m^3 during the first abandonment year, giving a maximum permeation flow of about 1.7 l/day/ m^2 through the VE-2 roof.

The above overview of consecutively investigated squeeze and migration processes clearly indicates that there is no need for significantly reducing the system's free brine volume prior to safe sealing and abandonment of the caverns.

Furthermore, it should be noticed that the free brine volume of $1.85 \cdot 10^6 \text{ m}^3$, left behind in a no bleed-off case, is completely defined by the very conservative standard bulking factor of 1.10 applied in the Winningsplan 2013q. As shown in Table 14, even 1 or 2% more rock bulking would result in significantly smaller amounts of squeezable free brine. This essential item, representing an epistemic uncertainty, is elaborated in more detail in Chapter 10.

Ad 5) Most critical parts of cavern system in view of sealing and abandonment

Attachment 13 shows an up-to-date true scale cross section of the shallowest parts of the cavern field, in which all structural elements are included and indicated that play a role in the cavern sealing and abandonment processes.

Casing shoe well VE-1

As explained in Chapter 6 the last cemented casing shoe of well VE-1 is situated nearest to the Lower Bunter formation and it is the shallowest position in the cavern field. Therefore, this shoe has initially been identified as the weakest cavern field point in view of cavern sealing and abandonment. On the other hand, well VE-1 has no lower 1b cavern and the 3b upper

cavern is hydraulically isolated from the other caverns in the field. Although a future direct connection between the upper 3b cavern of VE-1 and the rest of the field cannot completely be excluded, its probability is deemed low based on the facts that well VE-1 is definitely inactivated because of its sensitive shallow casing shoe and that Nedmag has no further plans to actively produce salts from the 2b/3b carnallite layers in other wells.

Characteristic structure of dissolved 1b section

To date, the lower 1b caverns of wells VE-2 and VE-3 (not depicted in attachment 13) are mutually connected, but they are still isolated from the 1b lower caverns of VE-4 and the TR-wells. So, in that sense the cross section actually depicts a conservative situation in anticipation of possible future connections between the 1b caverns of VE-2 and VE-3 with those of VE-4 and TR-7.

The 1b section in the cavern field has the character of a so called ~~field~~ labyrinth. The cause of it lies in the strategy of ~~a~~ multi-well brining according to which water is injected in some wells and brine is produced from other wells. These activities are done in changing well configurations in order to obtain brine with a maximized $MgCl_2$ concentration.

This labyrinth is for the greater part, and in the near future possibly completely, filled with porous sump material consisting of insoluble material and precipitated salts not dissolvable in bischofitic brine. As shown before, even a bulking factor as low as 1.15 would within a couple of years completely choke the free volumes in the 1b section. The significantly reduced free brine volume still available in the system at final cavern abandonment would mainly be present in the old, inactive 3b caverns and would be subjected to little squeeze drive only.

Halite roof area 3b cavern VE-2

It has become evident from coupled balanced squeeze and permeation modeling that in case of strong post-abandonment squeeze drives the whole shallowly positioned Zechstein roof region of the cavern system is not tight anymore and can fairly easily transmit brine to the Lower Bunter mudstone. Via a typical modeling example it has been demonstrated that the squeeze and migration processes become physically more plausible by assuming that the shallowest positioned roof area of the VE-2 3b-cavern starts leaking integrally.

Additionally, it is not logical to just restrict the leaking area to the 3b cavern roof of VE-2 only. This statement is based on two considerations:

- The positive effective brine pressure relative to local lithostatic pressure is not confined to the roof area of the VE-2 3b-cavern, as a consequence of which far more Zechstein salt roof volume is subjected to brine permeation stimulating pressures.
- The sizes of the 3b cavern roof areas so far applied (see Chapter 5 and item 3 of Chapter 9) do likely not represent the real roof status in the mine. Typically, the BDS data based roof span of the VE-2 3b-cavern varies between 122 m and 132 m, whereas roof spans of other caverns even amount to figures of up to 400 m. Data obtained from in-situ sonar measurements, albeit scarce data, do not confirm these large BDS based spans.

Real size of 3b cavern roofs

Attachment 14 shows the most recent sonar measurement in a 3b-cavern. The sonar was run in 3b cavern TR-6 in February 2014 (ref.39) to investigate the status of the halite roof. The maximum roof span detected is 80 m. This number stands in sharp contrast to the BDS based TR-6 spans of 140 m to 260 m, given in Tables 7 and 15. Other 3b cavern sonars were run in TR-2 and TR-3 in May 1991. Roof spans of 85 m and 50 m, respectively, were detected. After 1991 more salt was produced from these caverns, so comparison with the diameters given in Tables 7 and 15 is with a proviso. To date, no more 3b cavern sonars have been run.

Even when keeping in mind that the sound waves of the measurement tool cannot precisely detect the jagged and rough edges of the caverns, the difference between practice and calculated figures is simply too big.

At least, one conclusion to be drawn is that using BDS based spans in stability and permeation analyses is a very conservative approach. A more challenging conclusion is that application of unrealistic span numbers may lead to erroneous or ineffective measures in view of guaranteeing long-term mining practice with minimal potential damage to third parties.

10 Assessment of bulking factors from a literature survey

The study of the bulking factor is a condition of the approved ~~W~~Winningsplan 2013q(Article 4, Letter of Approval from the Minister of Economic Affairs, 3 October 2014).

Since the remainder of the cavern system's free brine volume is very sensitive to 1% more or less bulking of the insoluble materials, a relevant range of bulking factors is assessed based on a literature survey.

Most literature on bulking factors of materials is related to surface excavation, underground hard rock mining and mining by means of caving methods. The bulking process in the case of Nedmag, however, occurs *within* a salt formation as a result of solution mining that sets free insoluble bulking materials, while salt is being dissolved.

The pertinent literature in the SMRI library has been investigated. Most published data on bulking factors are related to the formation of sinkholes above unstable shallow caverns. In fact, such phenomenon can be characterised as a bulking process caused by caving, not by solution mining.

Bulking process inside salt formation caused by solution mining

The following SMRI information on bulking factors, pertaining to solution processes *inside* salt layers that contain appreciable amounts of insoluble material, has been found (refs.31-34):

- Dussaud (ref.31): cavern TS27: bulking factor 1.5, average insoluble content 27%. Model-derived cavern and sump growth coincided very well with sonar measurement results.
- Hellberg (ref.32): cavern Kiel 102, insoluble volume 22.6%, *assumed* bulking factor 1.6. Combining information from the publications Figure 4 (Geology) and 6 (Sonar survey after leaching 270000 m³ without sump) enables an assessment of the effective bulking factor. The bulked sump is assumed to have a height of 60 m and an average diameter of 50 m, giving a bulked sump volume of 120000 m³ and a disturbed formation total volume of 390000 m³. The disturbed, insoluble net volume is 87750 m³ (22.5%). In order to get the calculated bulked sump volume an effective bulking factor of circa 1.4 has to be applied.
- Charnavel (ref.33): the bulking factor is set to 1.5 and an insoluble content varying per 0.5 m is applied. For cavern EZ16 a leaching simulation program yielded bulked sump dimensions somewhat smaller than measured by sonar surveys. It is not clear, however, whether this is caused by an underestimated insoluble percentage or too low a bulking factor.
- Boor (ref.34): this publication on building gas storage cavern TGC-2 contains a rock-mechanical review of IfG, Leipzig (Institut für Gebirgsmechanik). Dominant non-salt layers were destroyed by intensively leaching the surrounding and intermingled salts. Unfortunately, specific data on the average insoluble content, the bulking factor and the relative volumetric dimension of the sump were not published. A request for providing this information on TGC-2 and, preferably also on wider IfG experience with bulking factors, has been sent to D. Brückner of IfG in Leipzig.

The following answer has been received from IfG per email of 17 July 2014:

- As far as the general range of bulking factors is concerned, according to IfG experiences the factor is between 1.3 and 1.5. It depends on the deposit and the content and the distribution of insoluble.
- From cavern projects in *Germany* it is known that anhydrite mostly consists of finely distributed particles between the salt grains, in which case a factor 1.5 is more common.

The factor is step by step reduced, if the distribution is coarser. Generally, the anhydrite content ranges between 2 and 10 %. In the case of higher content massive anhydrite grains or bands are encountered.

- As far as claystone is concerned, the bulking factor for the Haselgebirge salt formation with a mean claystone content of up to more than 20 % is also in the range of 1.3, because massive claystone is coarsely inter-bedded into a halite matrix.
- Deduced from the experiences IfG expects a bulking factor less than 1.3 for inter-bedded strata of anhydrite or dolomite because they are insoluble. If salt-healed fractures are dissolved, massive blocks of those materials fall into the sump without any bulking, reducing the bulking factor to the lower limit of 1.

Bulking factor of rock layers above unstable caverns

Many SMRI publications deal with sinkhole occurrences above unstable caverns. The bulking factors published are characteristic of the overburden material, which is usually not made up of salt. The overlying formations are normally not leached, but become mechanically overstressed and, subsequently, collapse into the cavern space.

A typical example of caving in the Netherlands is found in the Akzo Nobel cavern field in Hengelo (refs.35, 36). The amount of observed caving and subsidence above the unstable Hengelo caverns is indicative of *effective* bulking factors for the overlying Top Anhydrite and Röt claystone in the range between 1.07 and 1.11 only. The normally applied standard bulking factors for anhydrite, claystone and shale are far higher, in the order of 1.4 to 1.55 (ref.37).

However, in a reference publication on bulking factors of rock material (ref.38) it is explained why a big difference may occur between the bulking factor of a fully caved material and the *in-situ* bulking factor in a practical situation.

In long wall coal mining the caved rock behind the advancing long wall face is known as the *gob*. The bulking of the gob is affected by the fall height, as well as the size and shape of the rock fragments. When the fall height is larger than the lateral dimension of the rock fragments, the fragments are more likely to rotate and come to rest in an open disorderly arrangement with large void ratio. As caving proceeds upward, the caved rock occupies a progressively increasing proportion of the free space, thus reducing the fall height of the subsequent fragments. The potential for fragments to rotate diminishes and the amount of bulking is reduced.

In the Hengelo cavern field it has been observed by sonar measurements in some unstable caverns and in a dedicated exploration well into a subsided cavern area that the overlying rock layers have often failed in single events with almost no crumbling and bulking phenomenon. Thus, the large detached fragments have not rotated, which explains the observed very small *in-situ* bulking factors.

This observation of caving with reduced bulking factors above unstable caverns is in line with the above experiences of IfG in case of cavern leaching. If salt-healed fractures in anhydrite or dolomite in the salt formation are dissolved, massive blocks of those materials fall into the sump without any bulking, reducing the bulking factor to values near the lower limit of 1.

Discussion

In view of the results of the above literature study it seems less adequate to adopt Akzo-derived bulking factors, since they are related to an incomparable process of collapsing and

bulking bedded overburden rock. Thus, the applied realistic bulking factor of 1.10 as the base case of Nedmag's Winingsplan 2013 is not supported by the collected data so far.

Only if the presence of massive undissolved blocks or degraded non-tilted insoluble layers can be clearly demonstrated, this circumstance would definitely reduce the overall bulking factor to values below 1.3. This reduction is caused both by the lack of crumbling of the blocks and the filling of the voids in-between the blocks by finer insoluble particles or precipitated salt crystals. In other words, only a very inhomogeneous distribution of insoluble and precipitated particle sizes will effectively reduce the expected standard bulking factor. This condition is not very likely in the Nedmag mine, as dolomite and anhydrite sediments do not exist in the ZE-III salt layers from which the magnesium salts are produced and, therefore, the presence of large non-crumbled pieces of material can be disregarded.

Compaction is another mechanism that might reduce the volume of the bulked insoluble material (the sump) and thus result in an apparently smaller bulking factor. If the initial bulking factor is 1.4, the brine-filled porosity of the sump is circa 28.5%. Loading of this porous material by the lithostatic pressure of the surrounding salts could compress the sump and reduce the porosity. During production the operational pressure deficit in the brine is held constant at 67.5 bars re lithostatic at a depth of 1463 m TV NAP (TR-7 shoe position). The average depth of the ZE-III-1b section from which the bischofite brine is produced is 1695 m TV. At this depth the operational pressure deficit amounts to circa 85 bars. The compaction coefficient of the porous sump material is unknown, but a constant load of 85 bars is a moderate load only. If in the long run it would reduce the porosity by a conservative factor of $\frac{1}{4}$, the porosity is still 21.4%. This corresponds to a reduced effective bulking factor of 1.27. After final abandonment of the mine the enclosed brine pressure will increase to almost lithostatic values and the sump gets unloaded. This will halt any further sump compaction.

Recommendation

For Nedmag, only the bulking process *inside* the salt formation is relevant (ZE III-1b and 2b/3b salt layers). Then, according to the collected information and in view of the items discussed above, realistic bulking factors in the order of 1.4 to 1.5 should be applied for finely-distributed insoluble components.

In case of proven coarser insoluble material in the salt a more conservative bulking factor of 1.3 might be adopted (giving an initial 23% porosity of the bulked sump).

11 Summary of principal abandonment modeling results

Before considering the possible implications of the above analyses for abandonment scenarios the main results are summarized point by point:

1. In all operational phases (production, pre-abandonment bleed-off and final abandonment) the two-branch squeeze model, incorporating both non-linear and linear salt creep mechanisms, should be used.
2. Based on BDS volumes as calibration reference and BDS control parameters, optimum multi-salt modeling is achieved with relative mobility factors 1 (halite), 40 (carnallite) and 160 (bischofite).
3. During all operational phases roof stability is warranted for all caverns.
4. In fact, free-brine bleed-off at reduced cavern pressures in preparation of definite cavern sealing and abandonment is not necessary for controlling long-term land subsidence.
5. Under abandonment conditions the two-branch squeeze model has to be integrally coupled into an equilibrium relation between cavern convergence, hydraulic roof capacity and the containment properties of the overlying permeable rock layer (Lower Bunter).
6. Discarding the pre-abandonment bleed-off phase and finally abandoning the complete cavern field with almost two million m³ of free brine in place is certainly allowed with respect to the Zechstein roof integrity and the containment capacity of the overlying Lower Bunter mudstone.
7. The Zechstein salt roof starts easily leaking under abandonment stress and pressure conditions - in other words, salt is not hydraulically tight anymore under abandonment conditions. Despite this fact the Lower Bunter containment process and capacity enables a safe long-term abandonment.
8. The huge containment capacity of the Lower Bunter mudstone, limiting the pore pressure increase to about 0.1 MPa, makes the overlying, very tight Solling claystone redundant as ultimate confinement zone and environmental barrier.
9. A literature survey on bulking factors indicates that the applied ~~realistic~~ bulking factor of 1.10 as base case of Nedmag's Winningsplan 2013 is not supported by the collected data so far. For Nedmag, only the bulking process *inside* the salt formation is relevant (ZE III-1b and 2b/3b salt layers). Then, in case of coarse insoluble material a (conservative) bulking factor of 1.3 seems appropriate and in case of finely-distributed insoluble components 1.4 or more should be applied.
10. For bulking factors > 1.2 the total cavern system in the 1b section must meanwhile be choked by insoluble material and precipitated salts. Likely, the 1b section forms a labyrinth of porous material with actual porosities between 25 . 30% (bulking factor 1.35). This situation is depicted in Attachment 13. Consequently, in reality the large free brine volumes announced in the Winningsplan 2013 probably do not exist.

Particularly, the issue of far too high free brine volumes presented in the Winningsplan 2013 has consequences for future operation scenarios. This topic is discussed in the next chapter

12 Production and abandonment scenarios

The preceding analyses have provided much insight into the key factors that control and determine the long-term abandonment processes in the Nedmag cavern field. Based on these findings it suffices to elaborate two production and abandonment scenarios only.

The consequences of the following two scenarios are inventoried and presented:

1. Mining activities according to Nedmag's Winningsplan 2013q including brine bleed-off periods before final cavern sealing and abandonment.
2. WEP proposal based on the present study: active brine production nearly up to the land subsidence limit of 65 cm, followed by hard shut-in of all wells without pre-abandonment bleed-off period.

Potential risks involved in the two scenarios are taken into account, as described in the previous chapters.

12.1 Scenario 1: Nedmag Winningsplan 2013

Summary of key elements in Winningsplan2013

In the next list the most important aspects of the Winningsplan 2013 plan are summarized:

- During active leaching the average cavern convergence is $0.35 \cdot 10^6 \text{ m}^3$, causing circa 2.2 cm per year land subsidence (criterion: 6.2 cm subsidence per 10^6 m^3).
- Active leaching is ended after $9.5 \cdot 10^6 \text{ m}^3$ of cavern convergence with an expected land subsidence of 59 cm at the end of the year 2023.
- The assumed bulking factor is 1.1 and the expected cavern-field free brine volume is $1.0 \cdot 10^6 \text{ m}^3$ at the start of a pre-abandonment bleed-off period in 2024.
- Expected bleed-off volume is $0.5 \cdot 10^6 \text{ m}^3$ of bischofitic brine in 3 years time.
- Expected bleed-off volume is $0.5 \cdot 10^6 \text{ m}^3$ of carnallitic brine in the following years.
- The total squeeze volume at the end of the bleed-off procedure is circa $10.5 \cdot 10^6 \text{ m}^3$ and the closed-in free brine volume at final abandonment is practically nil.
- Expected maximum final land subsidence due to salt production m65 cm.

WEP feedback on Nedmag's Winningsplan 2013

WEP has analysed Nedmag's planning and figures by means of BDS-based modeling. Using the two-branch squeeze model the following feedback on the Nedmag planning has resulted (see Table 5, base case):

- In case of an applied bulking factor of 1.10 active leaching has to end sooner than planned, namely at the end of 2021, after $8.44 \cdot 10^6 \text{ m}^3$ cavern convergence with a remaining free brine volume of $2.16 \cdot 10^6 \text{ m}^3$. The expected land subsidence is circa 51 cm (criterion: 6.0 cm subsidence per 10^6 m^3 squeeze).
- The pre-abandonment phase starts in the beginning of 2022. After a period of 10 years of pre-abandonment squeeze the remaining free brine volume is circa $0.17 \cdot 10^6 \text{ m}^3$ and the total squeeze volume is $10.43 \cdot 10^6 \text{ m}^3$, causing an expected land subsidence of 62.6 cm in 2032.
- In the first definite abandonment year 2032 the free brine permeation into the roof of the shallowest upper cavern VE-1 is circa 477 m^3 .
- In 2132, after 100 years of definite abandonment the total migration volume amounts to circa 40000 m^3 and the expected additional land subsidence is 2.5 mm.

From the rock mechanical and hydraulic sensitivity analysis of Chapter 9 it is evident that the risks involved in the Winningsplan 2013 are minimal. External safety is hardly an issue in view of this type of deep salt mining. The only consequence of the mining that represents potential nuisance and impact to third parties is land subsidence. With timely measures taken by Nedmag in cooperation with the competent authorities this problem can be satisfactorily mitigated and compensated.

12.2 Scenario 2: WEP proposal

A major conclusion from this study (see chapter 9) is that free-brine bleed-off in advance of definite cavern field abandonment is not necessary. Long-term land subsidence remains in control and the Zechstein roof integrity and the containment capacity of the overlying Lower Bunter mudstone are fit for purpose. The Solling claystone is not needed as ultimate confinement barrier for migrating brines.

Consequently, WEP has developed an alternative scenario for field abandonment, which also matches with BDS data. The main characteristics of scenario 2, the so-called *no bleed-off* case, are based on the results obtained from the calibrated balanced two-branch squeeze model presented in paragraph 8.3. The figures are as follows:

- Active brine production can be continued until end 2026 with total squeeze amounting to $10.13 \cdot 10^6 \text{ m}^3$ (from July 1993) and remaining free brine volume $1.64 \cdot 10^6 \text{ m}^3$ (using an operational bulking factor 1.10).
- The total cavern field is subjected to a hard shut-in operation at the beginning of 2027 without pre-abandonment period of bleeding-off free brine. The land subsidence at that moment in time is expected to be 60.8 cm.
- In the first definite abandonment year 2027 the free brine permeation into the roof of the 3b-cavern VE-2 is circa 7150 m^3 .
- In 2127, after 100 years of definite abandonment the total migration volume amounts to circa $0.4 \cdot 10^6 \text{ m}^3$ and the expected additional land subsidence is 2.5 cm, making a total of circa 63.3 cm.

Similar remarks as made on the absence of risks involved in the Winningsplan 2013 hold for the mining scenario without pre-abandonment bleed-off period. Here, external safety is hardly an issue as well. The amount and occurrence of land subsidence involved is identical to the Winningsplan 2013 scenario and identical are the timely measures to be taken by Nedmag.

12.3 Concluding remarks

In this study evidence has been produced that BDS data and pertinent figures in the Winningsplan 2013 for strategies of future brine production and cavern abandonment should be viewed with prudence.

Furthermore, in a separate study the observed difference between the squeeze volume obtained from the BDS material balance and the volume obtained by inversion of measured land subsidence will be investigated in more detail, as prescribed in Article 6 of the Letter of Approval Winningsplan 2013 from the Minister of Economic Affairs (3 October 2014).

For Nedmag land subsidence is a very important parameter. Therefore, it is of prime importance to acquire realistic and reliable estimations of land subsidence as a result of Nedmag's future salt mining. Crucial elements in this respect are the following:

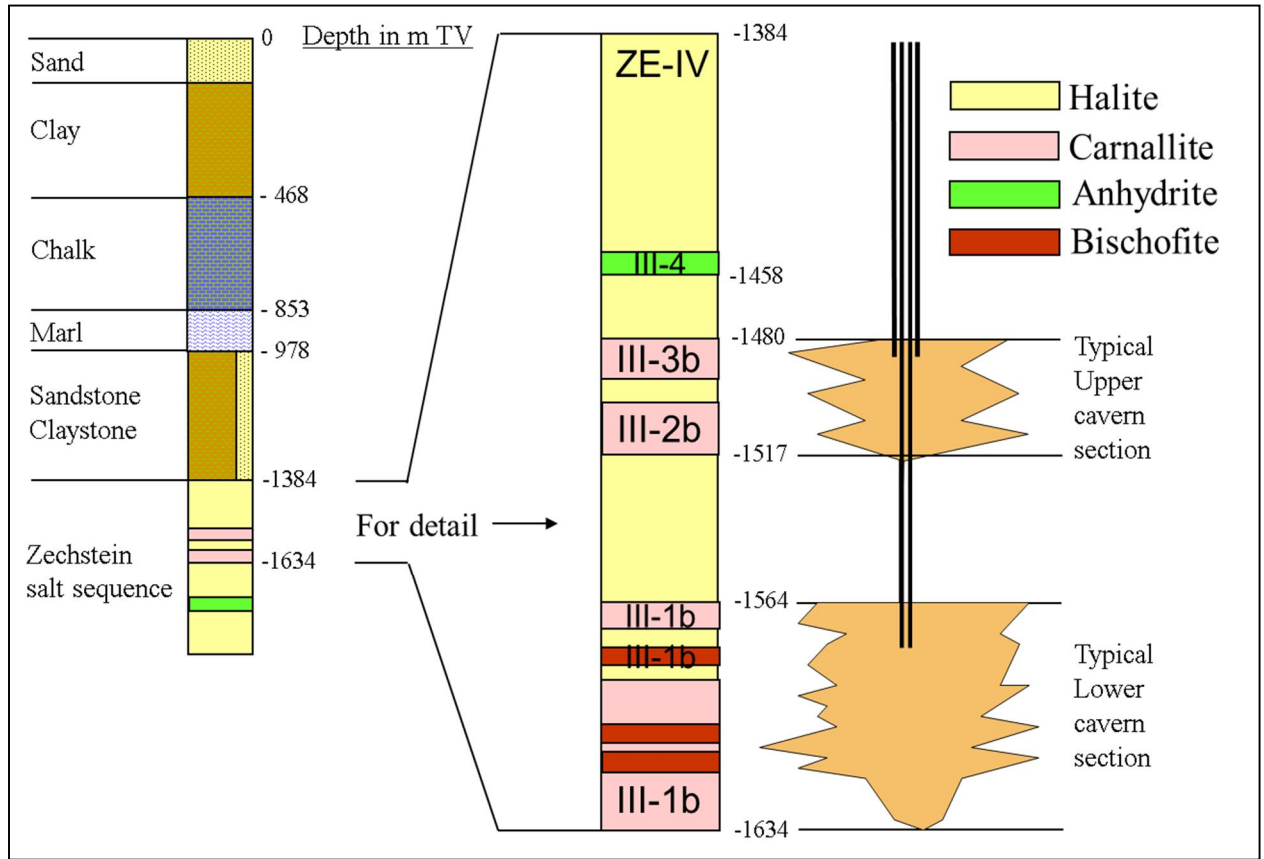
1. The concept of multiple well brining applies to the cavern field, according to which at the 1b ore level a diffuse labyrinth of dissolution channels is created and because of which it is impossible to reliably assign injection and production data to individual wells. Merely, a global modeling of the leaching process, both in time and place, is allowed.
2. The mine's bulking factors probably comply with standard figures worldwide in use for the type of inert rock material and salt precipitates involved in the Nedmag situation. This means that applying bulking factors below circa 1.20 should be considered as inadequate for determining free brine volumes.

13 References

1. Winningsplan kalium- en magnesiumzoutwinning 2013, Nedmag Industries Mining & Manufacturing B.V., Winningsvergunning Veendam, 26 maart 2013.
2. Controlestudie Frisia mijnmodel, J. Pruiksmā, Deltares, 9 april 2008.
3. Solution mining of magnesium-bearing salts in the Netherlands, D. Buyze et al., SMRI Fall Meeting, Kansas-City, 15-17 October 1984.
4. Creep of bischofite, H.A. van Eekelen et al., Proceedings 1st Conference on the Mechanical Behavior of Salt, State College, Pennsylvania, 9 -11 November 1981.
5. Shut-in gedrag en stabiliteit Frisia caveerne, J. Pruiksmā, GeoDelft rapport CO-400132-0006, v.2 def., juli 2005.
6. Solution mining magnesium salts by using a rock salt blanket, P.A. Fokker et al., SMRI Spring 1997 Meeting, Cracow, Poland, 11-14 May 1997.
7. Herziening opgeloste carnallietvolumes in 2b/3b cavernes, J.Visser, Nedmag Intern Memo, 5 februari 2015.
8. Casing shoe positions WHC-1 & WHC-2 2005, Nedmag Industries, 29 juni 2005.
9. Ronde schijven en platen, P. Hoogenboom, Sectie Constructiemechanica, TU Delft, februari 2008.
10. Bewertung frūherer Standsicherheitsuntersuchungen unter Einbeziehung aktueller Laborversuche an Kernmaterial der Bohrung 480, Abschlussbericht BGR, Hannover, Juni 2007.
11. Roof stability and integrity of cavern TR-4, WEP memorandum, Nedmag Industries, 1 December 2014.
12. Review of static and dynamic compressibility issues relating to deep underground caverns, P. Bérèst et al., Int.J.Rock Mech.Min.Sci, 36:1031-1049, 1999.
13. Permeability prediction based on fractal pore-space geometry, H. Pape et al., Geophysics, Vol.64, No.5, 1999.
14. The feasibility of CO₂ storage in the depleted P18-4 gas field offshore the Netherlands (the ROAD project), R. Arts et al., Int.J.Greenhouse Gas Control, 2012.
15. An assessment of carbon sequestration potential in the UK . Southern North Sea case study, M. Bentham, Tyndall Centre Working Paper No.85, January 2006.
16. The mechanical behaviour of anhydrite and the effect of deformation on permeability development . implications for caprock integrity during geological storage of CO₂, S. Hangx et al., Geophysics Research Abstracts, Vol.12, EGU2010-8181-1, 2010.
17. Literature review and recommendation of methods for measuring relative permeability of anhydrite from the Salado formation at the Waste Isolation Pilot Plant, R. Christiansen et al., Sandia Report 93-7074, August 1995.
18. Improvements in MIT ϕ for solution-mined caverns, L. van Sambeek et al., SMRI Research Project Report 2005-1, May 2005.
19. An in situ creep test in advance of abandoning a salt cavern, B. Brouard et al., SMRI Fall 2004 Conference,3-6 October 2004.
20. Definitieve afsluiting van caveerne BAS-3, v.1.def, esco/Frisia Zout B.V., 5 november 2014.
21. Zum langfristigen Tragverhalten von verschlossenen solegefūllten Salzkavernen . ein neuer Ansatz zu physikalischer Modellierung und numerischer Simulation. Theoretische und laborative Grundlagen, K.-H. Lux, Erdōl Erdgas Kohle, Vol. no. 11, 2005.
22. Zum langfristigen Tragverhalten von verschlossenen solegefūllten Salzkavernen . ein neuer Ansatz zu physikalischer Modellierung und numerischer Simulation. Rechnerische Analysen und grundlegende Erkenntnisse, K.-H. Lux, Erdōl Erdgas Kohle, Vol. no. 4, 2006.

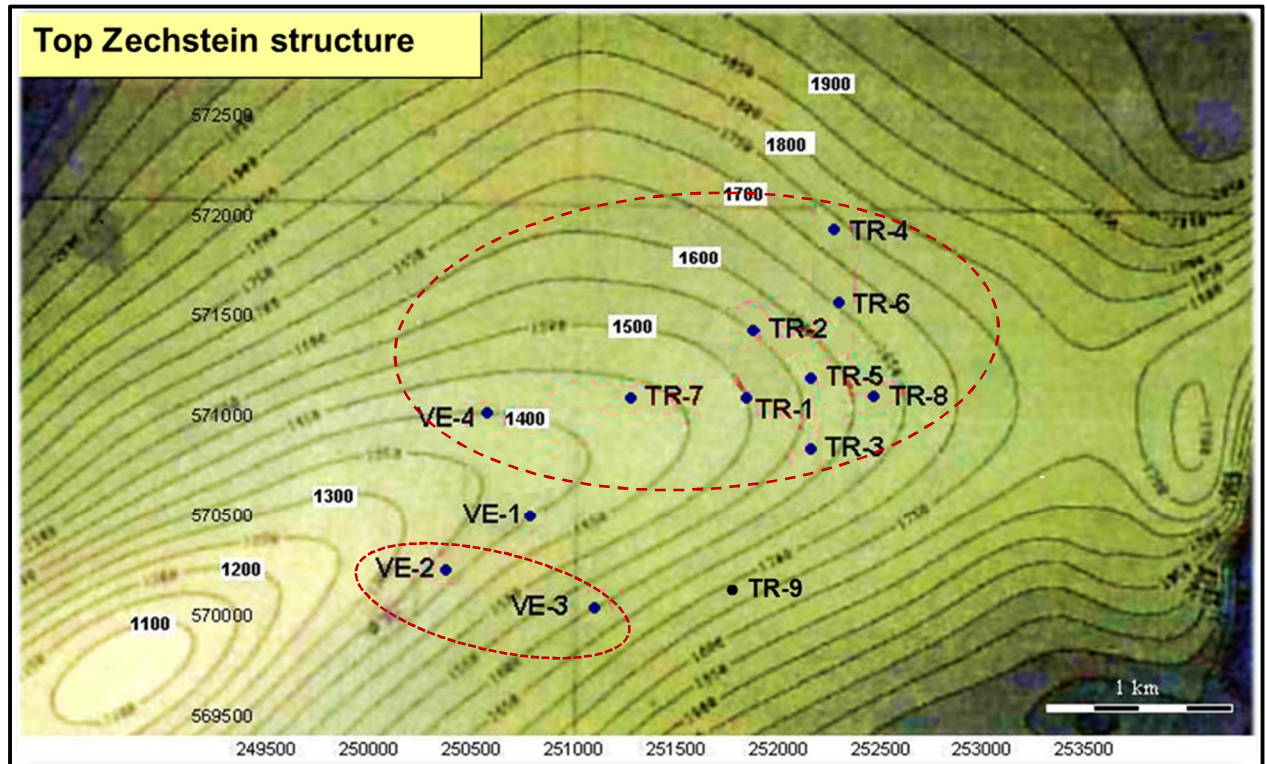
23. Long-term behaviour of sealed brine-filled cavities in rock salt mass . A new approach for physical modelling and numerical simulation, K.-H. Lux et al., SMRI Fall 2006 Conference, Rapid City, South Dakota, USA, 1-4 October 2006.
24. A salt-cavern abandonment test, P. Bérèst et al., SMRI Spring 1999 Meeting, Las Vegas, USA, April 1999
25. Applied rock mechanics (TA 4120 I), J.P.A. Roest, TU Delft, 2001.
26. Compressibility of sandstones, R.W. Zimmerman, Elsevier Science Publishers, Amsterdam, Netherlands, 1991.
27. Mudstone and claystone Units: seals for ancient microbial gas accumulations in the Upper Cretaceous MilkRiverformation, Alberta and Saskatchewan, N. Fishman et al., USGS Search and discovery article 10171, 2008.
28. Technisch geologisch onderzoek naar CO₂-opslag in het Barendrecht veld, S. Holt and M. Vasmel, Bachelor of Science eindschrijving TA3006, Delft, augustus 2009.
29. Geological foundation for production of natural gas from diverse shale formations, J. Pashin, Geological Survey of Alabama, Open file report 1110, Tuscaloosa, Alabama, August 2011.
30. In situ stress and permeability tests in the Hutchinson salt and the overlying shale, Kansas, Th. Doe et al., SMRI Fall 2006 Conference, Rapid City, South Dakota, USA, 1-4 October 2006.
31. Modeling and control of cavities development in a brine field, M. Dussaud et al., SMRI Fall Meeting 1990, Paris, France, 14-19 October 1990.
32. Construction of gas stores in salt with high insoluble fractions, C. Hellberg et al., SMRI Fall Meeting 1994, Hannover, Germany.
33. Insoluble deposit in salt cavern . Test Case, Y. Charnavel et al., SMRI Fall Meeting 2002, Bad Ischl, Austria, 6-9 October 2002.
34. Solution-mining with non-halites in Portugal, S. Boor et al., SMRI Spring 2012 Technical Conference, Regina, Saskatchewan, Canada, 23-24 April 2012.
35. Subsidence phenomena over solution cavities in bedded salt, Th. Wassmann, SMRI Fall 1995.Meeting, San Antonio, Texas, USA, 22-25 October 1995.
36. Stopping in weak rock over salt solution cavities in the Hengelo Brine Field, R. Bekendam, SMRI Spring 1997 Meeting, Cracow, Poland, 11-14 May 1997.
37. Assessment of sinkhole formation potential above brine caverns, M. Guarascio et al., SMRI Spring 1999 Meeting, Las Vegas, Nevada, USA, 11-14 April 1999.
38. Bulking Factor of Rock for Underground Openings, U.S. Nuclear Regulatory Commission, Contract NRC 02-07-006, G. Ofoegbu et al., February 2008.
39. Sonar echometry with lubricator, Nedmag cavity TR-6, Veendam, Flodim Report nr. 14-3015, 6 February 2014.
40. Bischofite creep tests and flow law, N. Muhammad et al., HPT Laboratory, Dept. Earth Sciences, Utrecht University, the Netherlands, August 2013.

Attachment 1: Stratigraphy of VE and TR subsurface



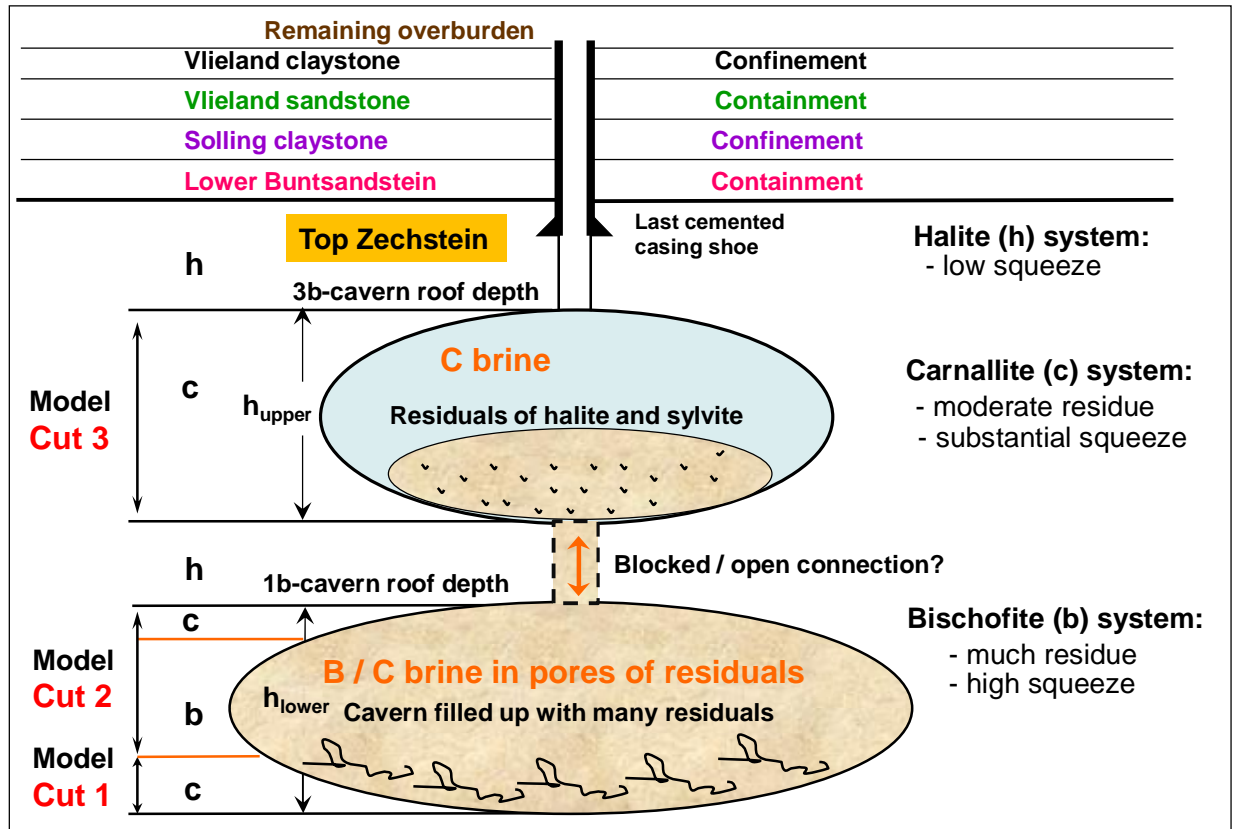
Zechstein-III salt formation and schematic position of Nedmag caverns.

Attachment 2: Map of Nedmag cavern system



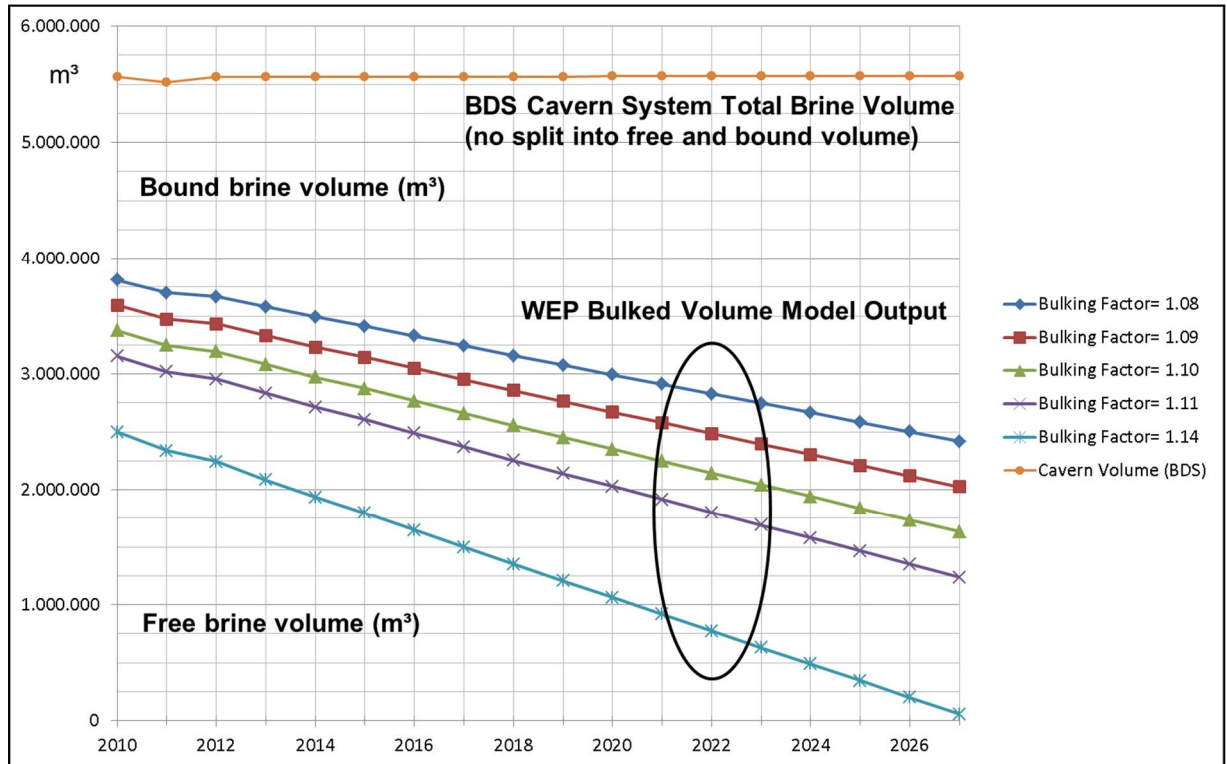
Positions of the 4 VE-wells and 9 TR-wells projected on the top of the Zechstein structure. The dotted red ovals indicate mutual cavern connections at the ZE-III-1b level.

Attachment 3: General cavern system model



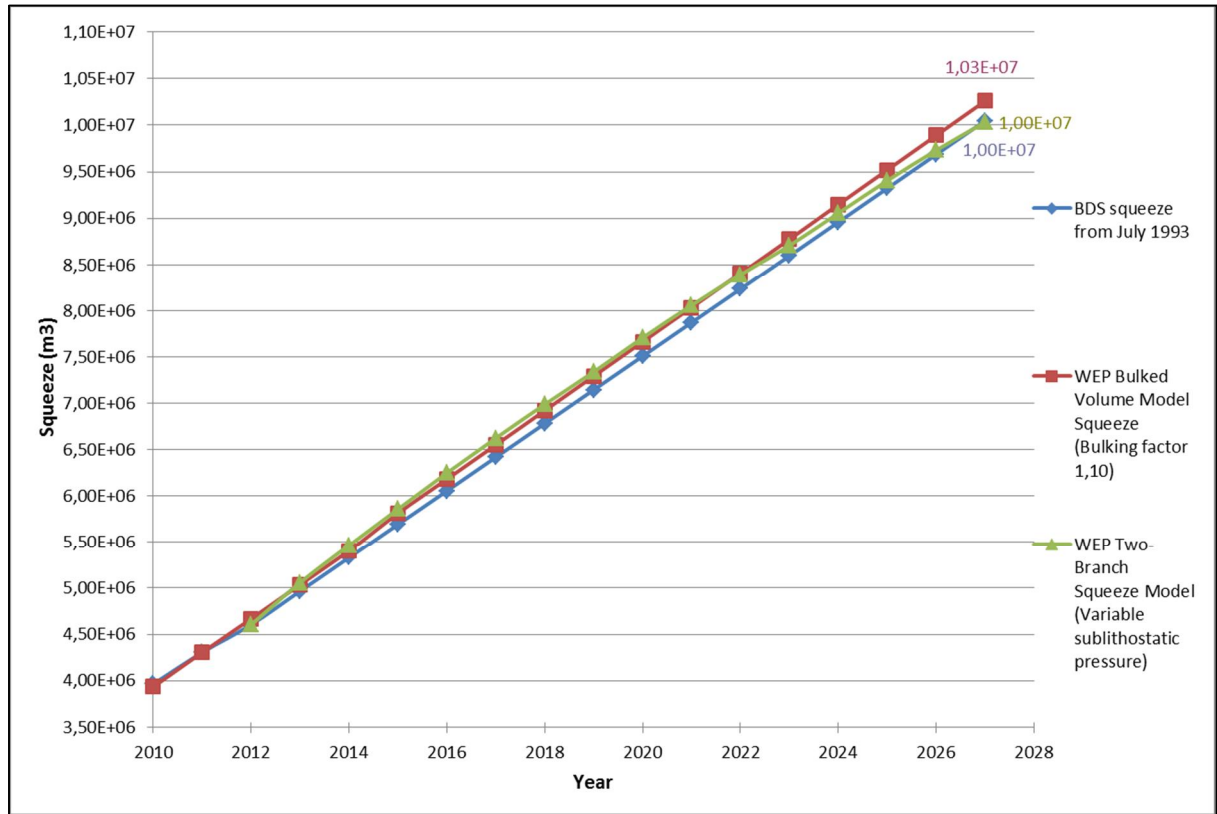
The lower 1b-section is divided into two cuts and the upper 2b/3b section consists of one cut.

Attachment 4: Bulked volume model output



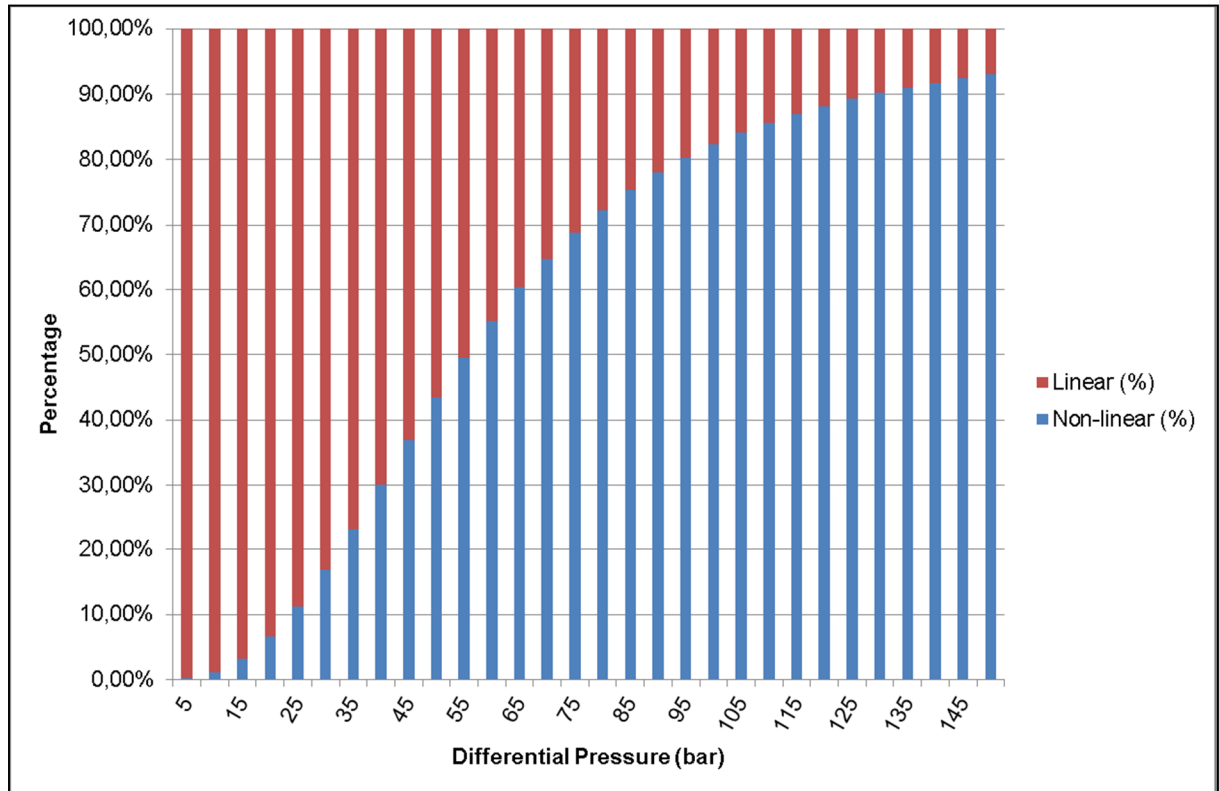
BDS cavern brine volumes are almost constant over the total time period 2010 - 2026. The WEP model splits the total BDS volumes into bound and freely movable fractions as a function of the bulking factor. In the Winningsplan 2013 the base case bulking factor is 1.10.

Attachment 5: Modeled squeeze volumes for production phase



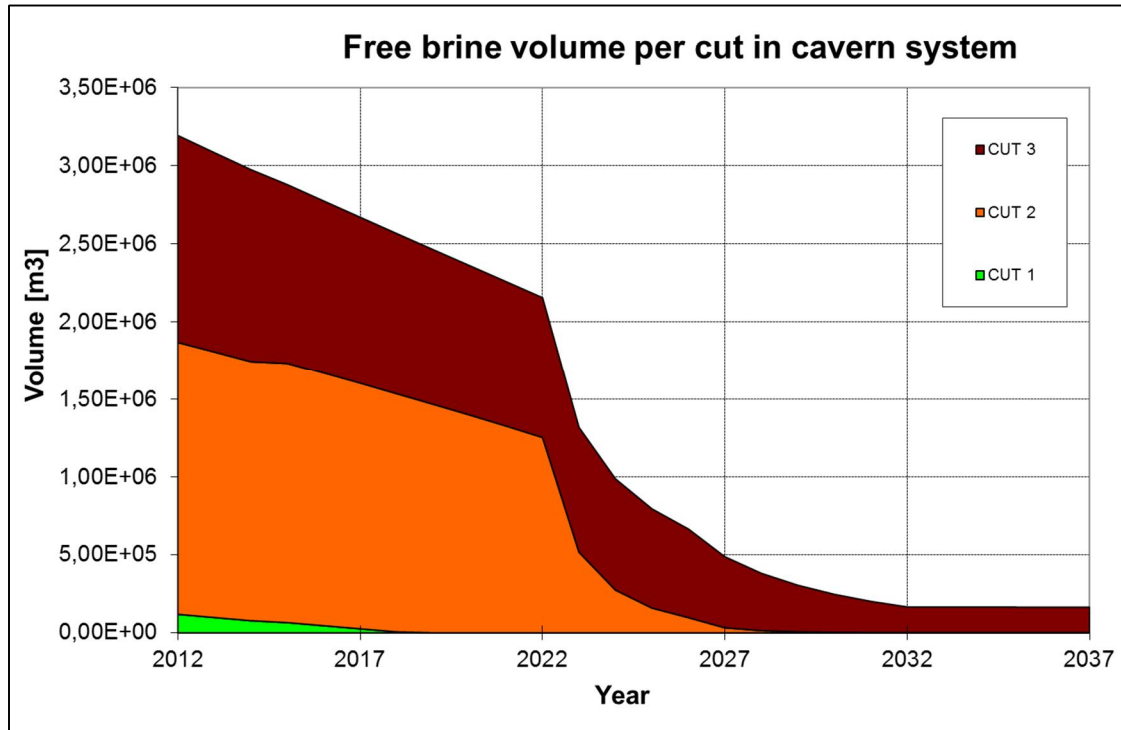
Similarity in the period 2010-2027 between the squeeze volumes of the two optimized WEP models and the BDS based cumulative squeeze volumes with reference date July 1993.

Attachment 6: Two branch relative squeeze contributions

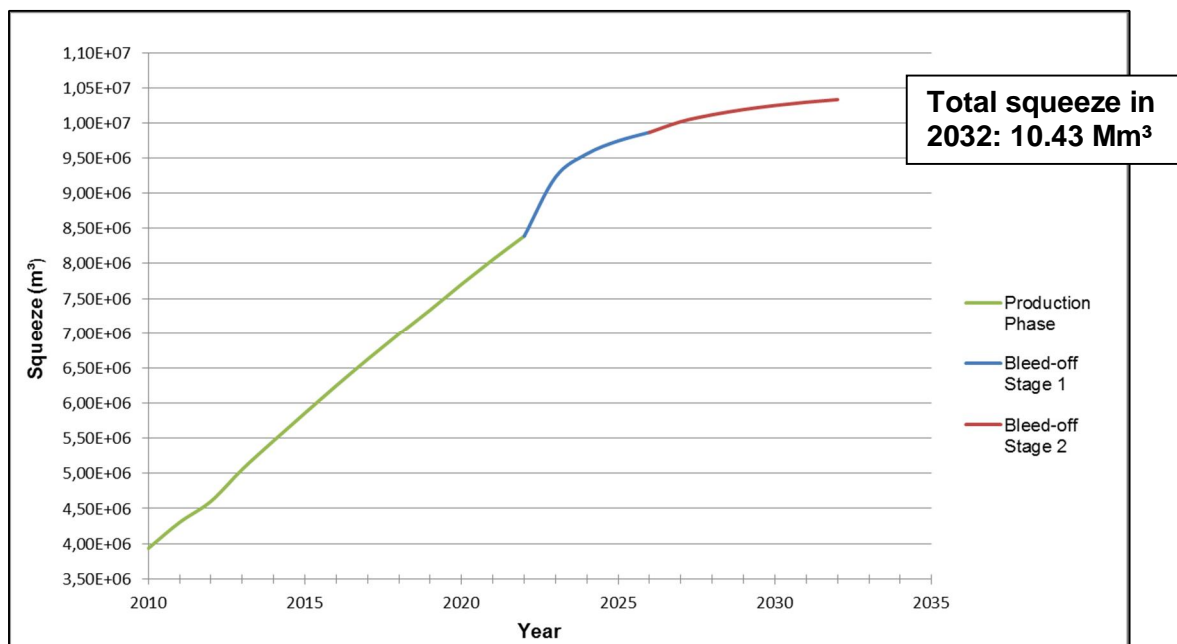


Percentage contribution of linear and non-linear salt creep to total cavern squeeze as a function of cavern brine pressure deficit, with $A_1 = 2.54 / \text{day} \cdot \text{MPa}^{3.6}$ and $A_2 = 9.0 / \text{day} \cdot \text{MPa}$ ($Q/R = 6201 \text{ K}$ and $T = 337.5 \text{ K}$).

Attachment 7: Free and squeeze volumes for production and pre-abandonment phase

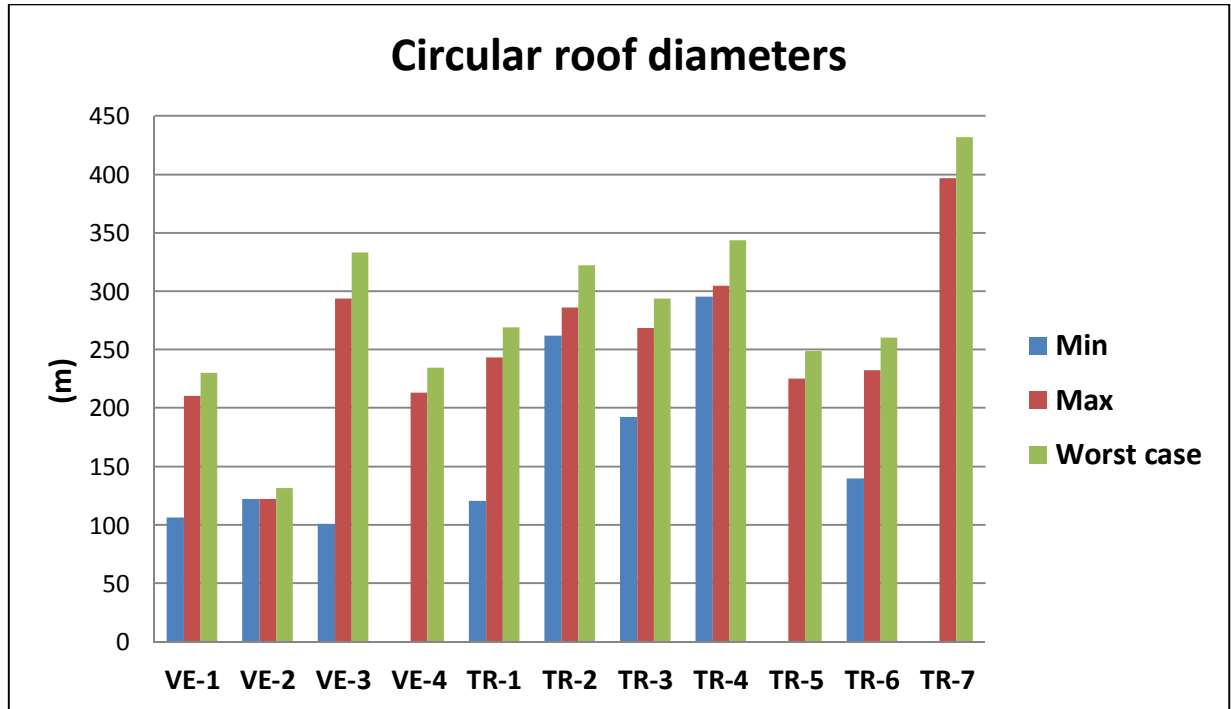


a) Decrease of total free volume in the three cavern system cuts. The pre-abandonment bleed-off phase starts at the beginning of 2022.



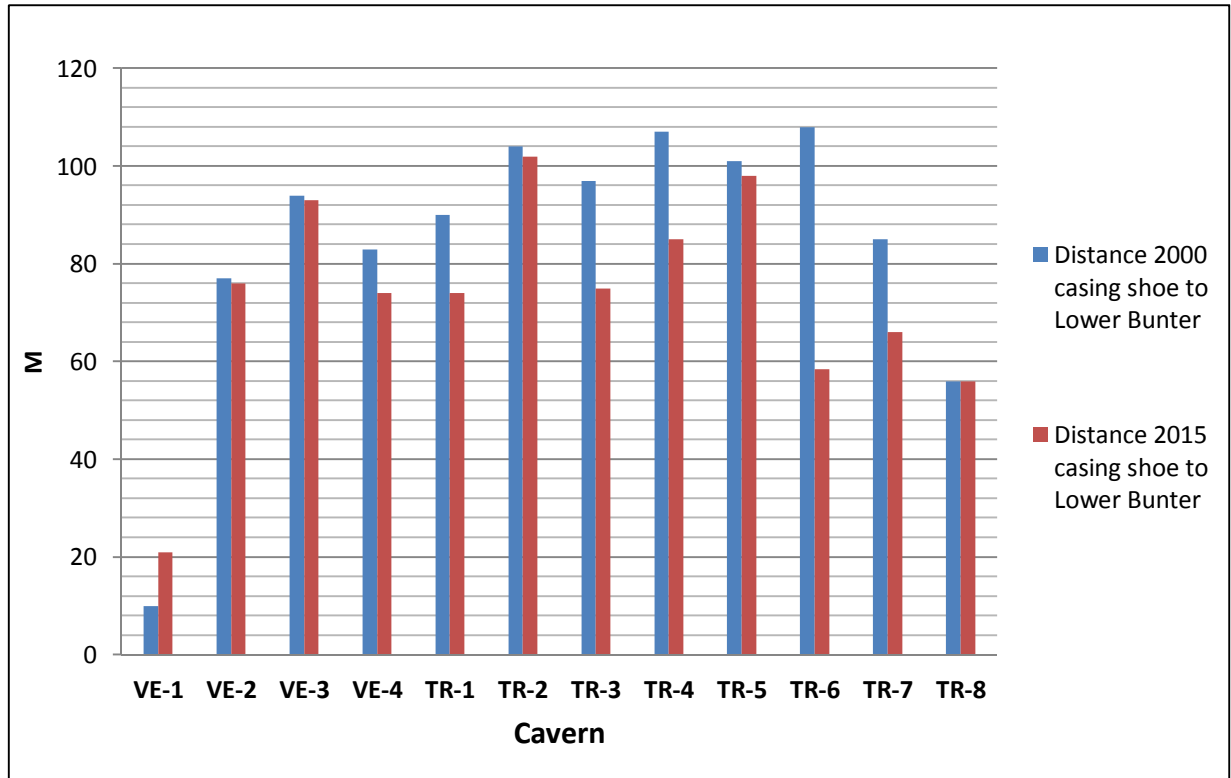
b) Increase of cumulative squeeze volume from the total cavern system. The bleed-off phase starts at the beginning of 2022.

Attachment 8: Equivalent circular span of 3b cavern roofs



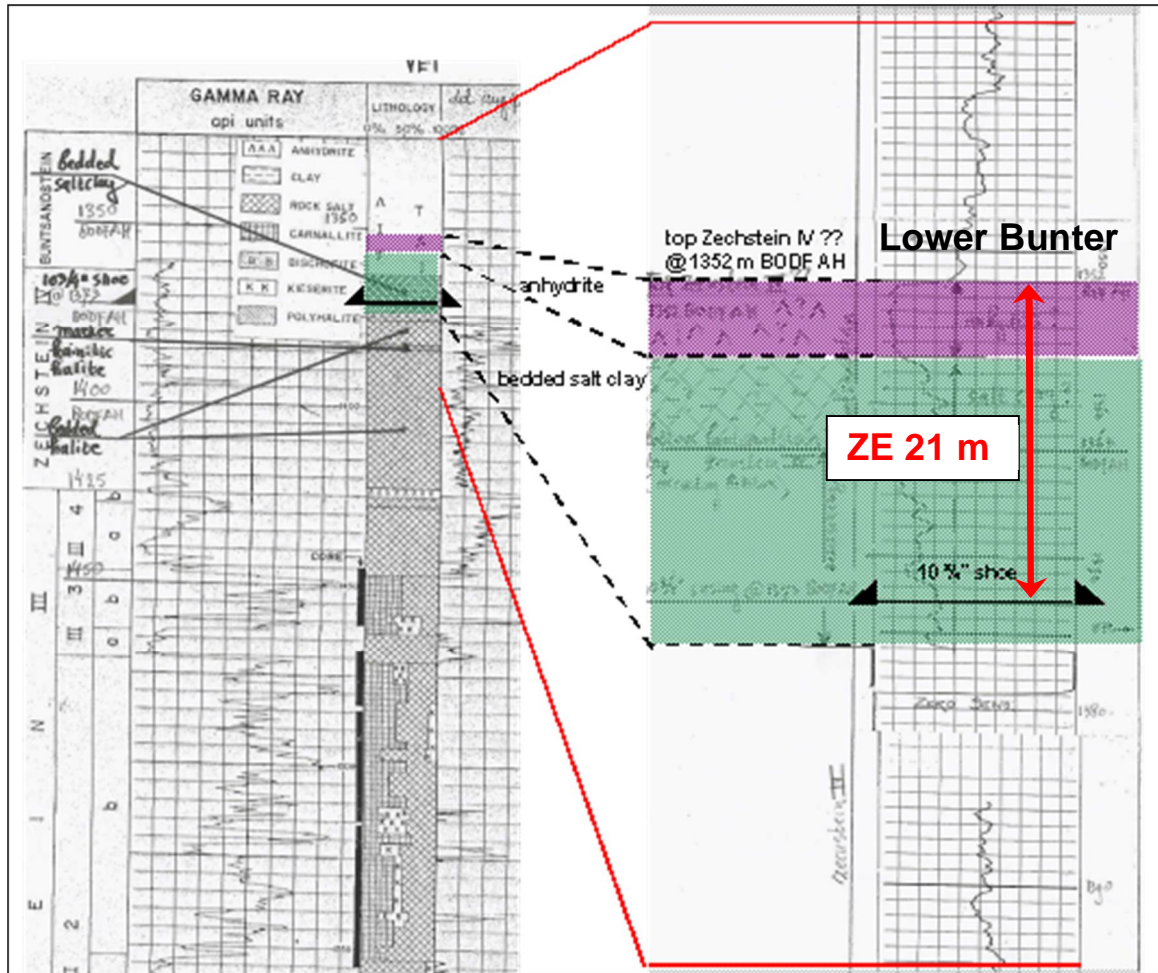
Cavern roof spans in the 3b-section transformed to a disc shape with minimum and maximum diameters as shown in the graph. Caverns TR-8 and TR-9 are not included, because they are only positioned in the lower 1b-section. The worst case values are derived in Chapter 9 and are based on cumulatively taking maximum uncertainties in input data into account.

Attachment 9: Salt barrier between 3b caverns and Lower Bunter formation



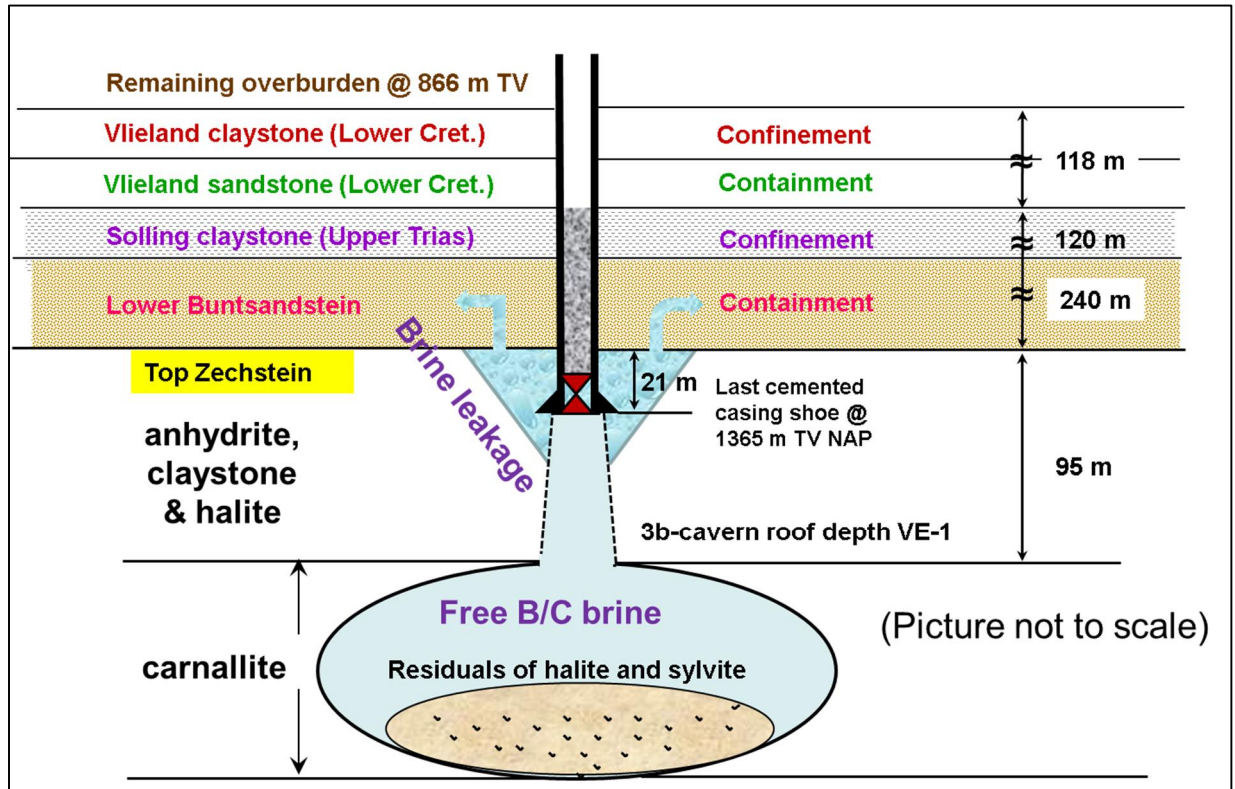
Change of distances between last cemented casing shoe and the overlying Lower Bunter mudstone (comparison between status in 2000 and in first quarter 2015).

Attachment 10: Roof composition near VE-1 casing shoe



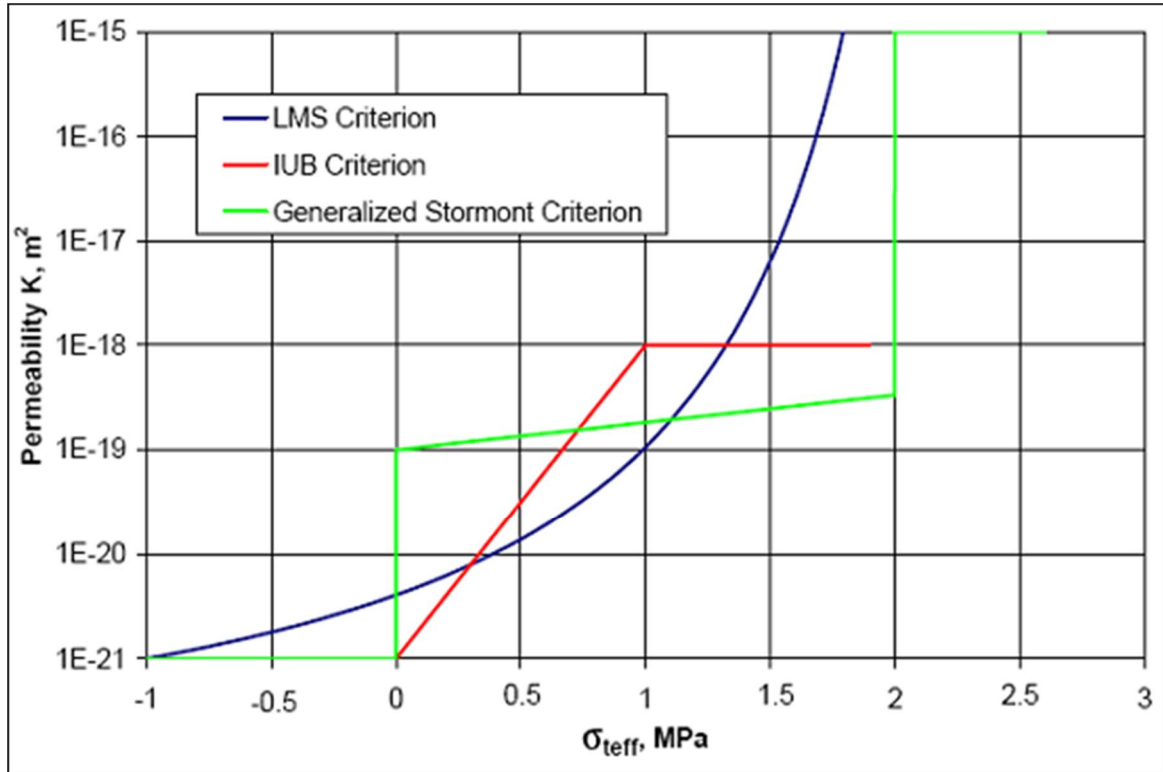
Log interpretation of roof composition near VE-1 shoe (ref.8). Shortest distance between shoe and Lower Bunter sandstone is 21 m. The 10³/₄+shoe is positioned at a depth of 1365 m TV NAP.

Attachment 11: Cavern situation VE-1 after abandonment



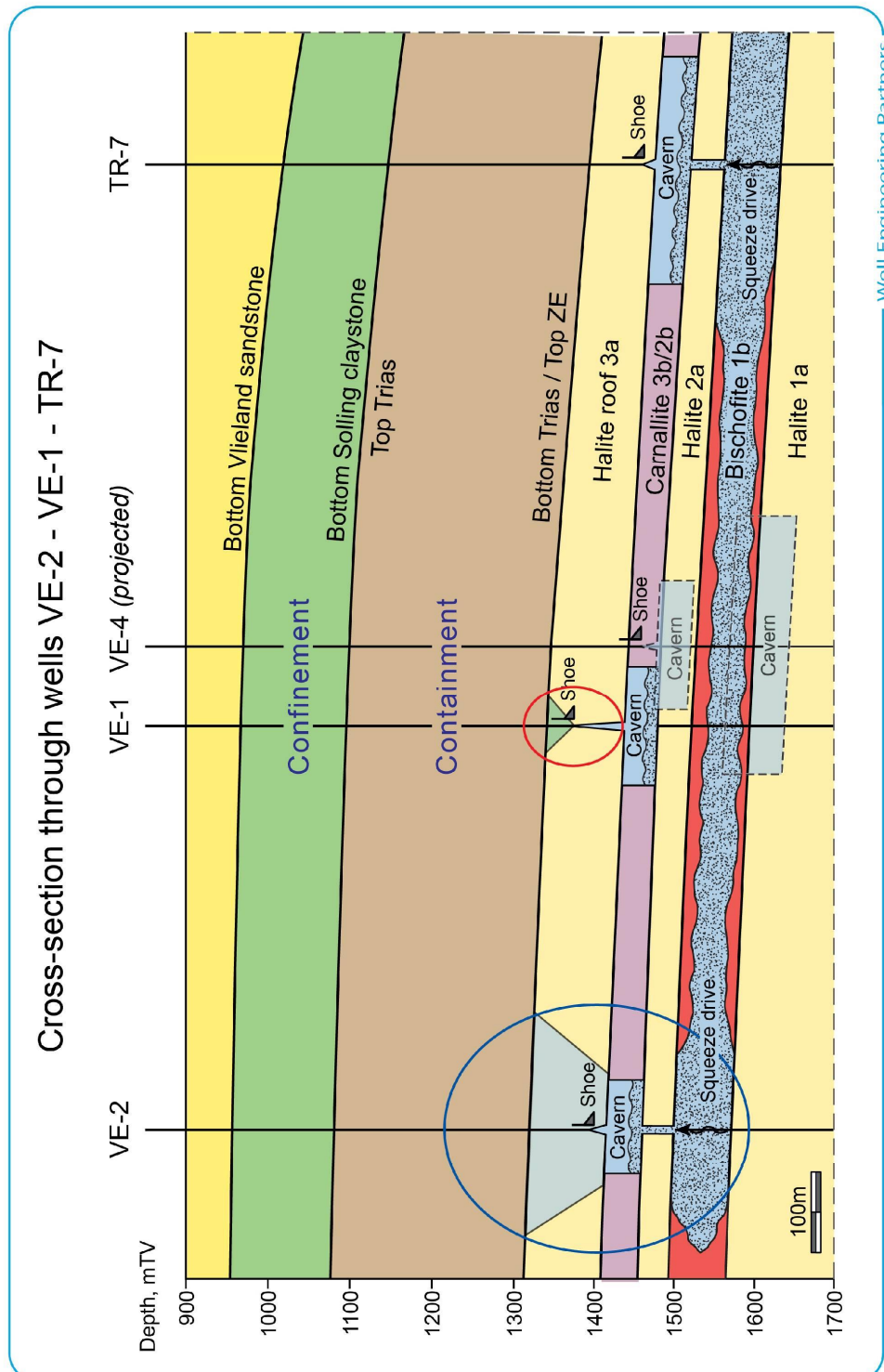
Well VE-1 is only connected to an upper cavern in the carnallite 3b section. The casing shoe at a depth of 1365 m TV NAP is the shallowest shoe in the cavern system.

Attachment 12: Halite permeability as a function of effective fluid pressure



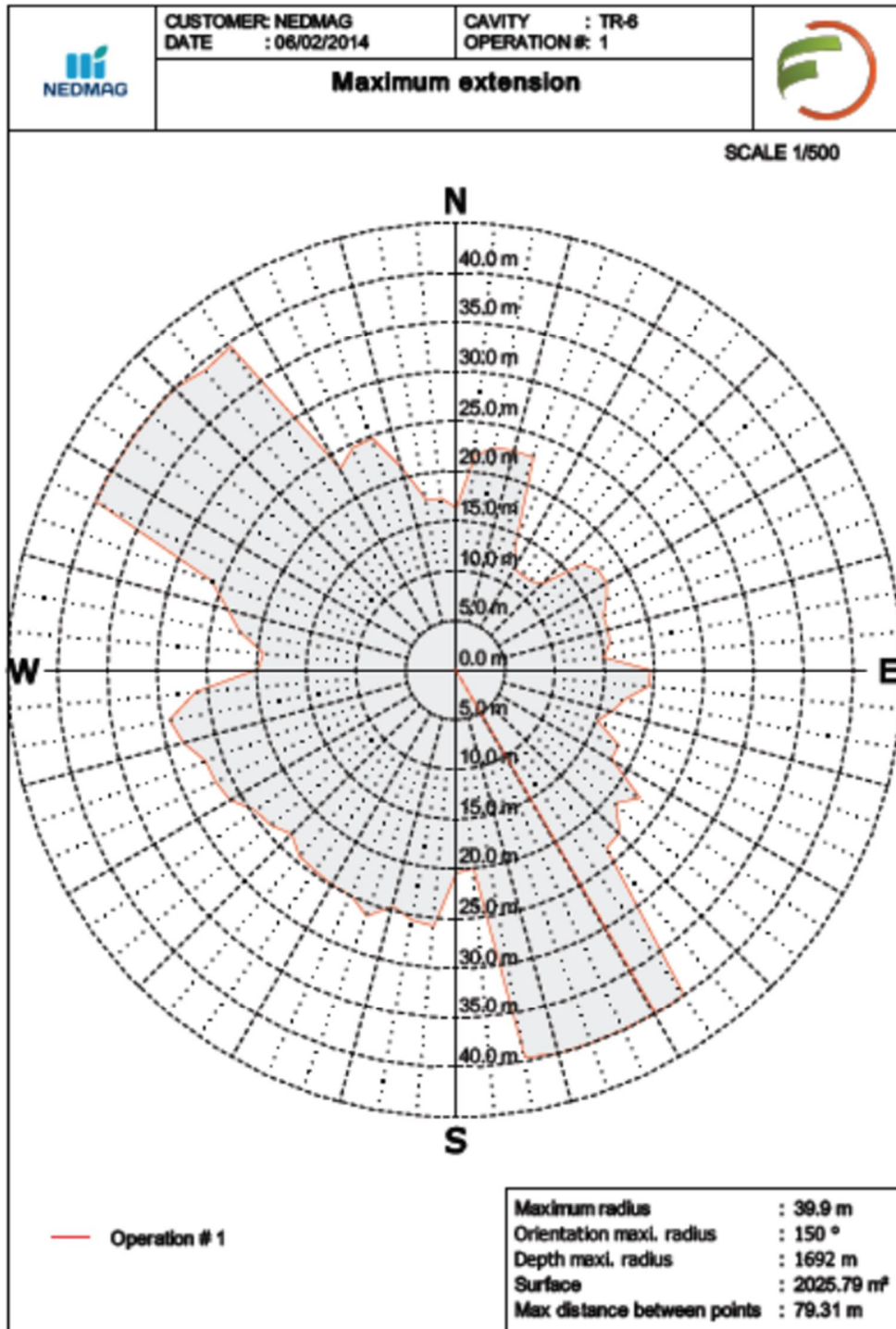
Different criteria for halite permeability as a function of effective stress $\sigma_{t,eff}$. Positive $\sigma_{t,eff}$ values represent local above-lithostatic brine pressure conditions

Attachment 13: Cross section through wells VE-2, VE-1 and TR-7



Upper and lower VE-4 caverns actually situated behind cross section, but projected and depicted somewhat blurred at the section. These caverns are positioned at depth levels equal to the TR-7 caverns. Also shown, integrally leaking VE-2 roof (blue circle) instead of VE-1 shoe alone (red circle). The overburden containment and confinement zones are also shown.

Attachment 14: Sonar measurement in 3b cavern TR-6



Maximum omnidirectional roof dimension of 3b-cavern TR-6 at a depth of circa 5 m below the halite roof. The 3b layer thickness is circa 8 m (cf. Table 7).

Attachment 15: Mohr-Coulomb stability criterion for disc-shaped roofs

Concept of cavern roof

The cavern roof is assumed to be a circular plate (disc), laterally clamped by a horizontal stress, loaded by the overburden weight and supported by the internal hydraulic cavern pressure.

In the center of the disc the stress pattern can be expressed as follows (ref.9):

$$\sigma_r = \sigma_\theta = \frac{3}{8} \cdot (1 + \nu) \cdot (R/h)^2 \cdot P_{\text{disc}}$$

with: σ_r = radial (tensile) stress
 σ_θ = tangential stress
 R = radius of disc
 h = thickness of disc
 ν = Poisson's ratio (halite 1/3, clay 1/4)
 P_{disc} = load of roof disc = $\gamma_{\text{ob}} \cdot H - P_{\text{cav}} = P_{\text{litho}} - P_{\text{cav}}$
 γ_{ob} = specific overburden weight
 H = roof depth (bottom side of disc)
 P_{cav} = internal cavern brine pressure at roof depth.

Mohr-Coulomb failure criterion

According to Coulomb the limit value for shear stress causing rock failure is as follows:

$$\tau = C + \sigma_n \cdot \tan \phi$$

with: τ = shear stress
 C = mechanical cohesion of rock (inherent shear strength)
 σ_n = normal stress perpendicular to failure plane
 ϕ = internal friction angle of rock.

The Mohr-Coulomb envelope gives the failure criterion in terms of principal stresses:

$$\frac{(\sigma_1 - \sigma_3)}{2} = C \cdot \cos \phi + \frac{(\sigma_1 + \sigma_3)}{2} \cdot \sin \phi$$

with: $\sigma_1 = \sigma_r = \sigma_\theta = \frac{3}{8} \cdot (1 + \nu) \cdot (R/h)^2 \cdot (\gamma_{\text{ob}} \cdot H - P_{\text{cav}})$
 $\sigma_3 = P_{\text{cav}}$

Inserting the expressions for σ_1 and σ_3 and solving for roof thickness h yields as criterion for roof stability:

$$h > 0.5 R \cdot \sqrt{\frac{[3/2 \cdot (1 + \nu) \cdot (\gamma_{\text{ob}} \cdot H - P_{\text{cav}}) \cdot (1 - \sin \phi)]}{[2C \cdot \cos \phi + P_{\text{cav}} \cdot (1 + \sin \phi)]}}$$

For salt rock $\nu = 1/3$ and substituting $(\gamma_{\text{ob}} \cdot H - P_{\text{cav}}) = \Delta P =$ brine pressure deficit re P_{litho} gives:

$$h > 0.5 R \cdot \sqrt{\frac{[2 \cdot \Delta P \cdot (1 - \sin \phi)]}{[2C \cdot \cos \phi + P_{\text{cav}} \cdot (1 + \sin \phi)]}}$$